

CHARACTERISTICS AND CATALYTIC PROPERTIES OF COPPER ON MCF-Si AND SBA-15  
FOR HYDROGENATION OF CARBON DIOXIDE



A Thesis Submitted in Partial Fulfillment of the Requirements  
for the Degree of Master of Engineering in Chemical Engineering

Department of Chemical Engineering

FACULTY OF ENGINEERING

Chulalongkorn University

Academic Year 2022

Copyright of Chulalongkorn University

คุณลักษณะและสมบัติการเป็นตัวเร่งปฏิกิริยาของทองแดงบน MCF-Si และ SBA-15  
สำหรับไฮโดรจิเนชันของคาร์บอนไดออกไซด์



วิทยานิพนธ์นี้เป็นส่วนหนึ่งของการศึกษาตามหลักสูตรปริญญาวิศวกรรมศาสตรมหาบัณฑิต  
สาขาวิชาวิศวกรรมเคมี ภาควิชาวิศวกรรมเคมี  
คณะวิศวกรรมศาสตร์ จุฬาลงกรณ์มหาวิทยาลัย  
ปีการศึกษา 2565  
ลิขสิทธิ์ของจุฬาลงกรณ์มหาวิทยาลัย

Thesis Title	CHARACTERISTICS AND CATALYTIC PROPERTIES OF COPPER ON MCF-Si AND SBA-15 FOR HYDROGENATION OF CARBON DIOXIDE
By	Miss Sirimas Suelueam
Field of Study	Chemical Engineering
Thesis Advisor	Professor BUNJERD JONGSOMJIT, Ph.D.

---

Accepted by the FACULTY OF ENGINEERING, Chulalongkorn University in  
Partial Fulfillment of the Requirement for the Master of Engineering

----- Dean of the FACULTY OF  
ENGINEERING  
(Professor SUPOT TEACHAVORASINSKUN, Ph.D.)

THESIS COMMITTEE

----- Chairman  
(Professor PIYASAN PRASERTHDAM, Ph.D.)

----- Thesis Advisor  
(Professor BUNJERD JONGSOMJIT, Ph.D.)

----- Examiner  
(Professor JOONGJAI PANPRANOT, Ph.D.)

----- External Examiner  
(Associate Professor Ekrachan Chaichana, Ph.D.)

สิริมาส ชื่อเลื่อม : คุณลักษณะและสมบัติการเป็นตัวเร่งปฏิกิริยาของทองแดงบน MCF-Si และ SBA-15 สำหรับไฮโดรจิเนชันของคาร์บอนไดออกไซด์. ( CHARACTERISTICS AND CATALYTIC PROPERTIES OF COPPER ON MCF-Si AND SBA-15 FOR HYDROGENATION OF CARBON DIOXIDE ) อ.ที่ปรึกษาหลัก : ศ. ดร.บรรเจิด จงสมจิตร

ในปัจจุบันการผลิตเมทานอลจากปฏิกิริยาไฮโดรจิเนชันของคาร์บอนไดออกไซด์เป็นไปอย่างแพร่หลาย ตัวเร่งปฏิกิริยาที่นิยมใช้ปัจจุบันได้แก่ตัวเร่งปฏิกิริยาคอปเปอร์ออกไซด์ ซิงค์ออกไซด์ และอะลูมิเนียมออกไซด์ (CZA) ซึ่งเมื่อปฏิกิริยาดำเนินไปตัวเร่งปฏิกิริยาจะเกิดโค้กขึ้น ทำให้ประสิทธิภาพของตัวเร่งปฏิกิริยาลดลง ในงานวิจัยนี้จึงศึกษาเกี่ยวกับตัวเร่งปฏิกิริยาคอปเปอร์บนตัวรองรับเมโซพอร์สซิลิกา ซึ่งตัวรองรับชนิดนี้จะมีเสถียรภาพทางความร้อนสูง โดยทำการสังเคราะห์ตัวเร่งปฏิกิริยาคอปเปอร์บนตัวรองรับ MCF-Si และ SBA-15 ซึ่งเป็นตัวรองรับเมโซพอร์สที่มีสัณฐานของรูพรุนแตกต่างกันโดยมีทรงกลมและทรงหกเหลี่ยมตามลำดับ ด้วยวิธีการเคลือบฝังแบบเปียก (wetness impregnation (W)) และ การเคลือบฝังแบบเอ็บซุ่ม (incipient wetness impregnation (IW)) โดยมีอัตราส่วนน้ำหนักของคอปเปอร์ที่ 60 wt% จากนั้นนำตัวเร่งปฏิกิริยาที่สังเคราะห์ขึ้นมาไปวิเคราะห์ลักษณะทางกายภาพและทางเคมีด้วยวิธี SEM-EDX, XRF, XRD, TEM, N<sub>2</sub> physisorption, TGA, CO-chemisorption และ H<sub>2</sub>-TPR พบว่า การฝังโลหะลงบนตัวรองรับด้วยวิธีทั้งสองไม่ทำให้ลักษณะโครงสร้างของตัวรองรับเปลี่ยนแปลงไป ก่อนจะนำตัวเร่งปฏิกิริยาไปทำปฏิกิริยาไฮโดรจิเนชันด้วยแก๊สคาร์บอนไดออกไซด์และไฮโดรเจนโดยจะแบ่งปฏิกิริยาเป็น 2 ช่วงคือ ช่วงแรกจะทำปฏิกิริยาที่อุณหภูมิ 100-400 องศาเซลเซียส ความดัน 10 บาร์ เพื่อศึกษาอุณหภูมิที่เหมาะสมในการทำปฏิกิริยาด้วยเร่งปฏิกิริยาชนิดต่างๆ พบว่าที่อุณหภูมิ 300 องศาเซลเซียส ตัวเร่งปฏิกิริยาที่ถูกรองรับด้วย MCF-Si มีอัตราส่วนของเมทานอลเกิดขึ้นมากที่สุด และที่ 400 องศาเซลเซียส ตัวเร่งปฏิกิริยาที่ถูกรองรับด้วย SBA-15 มีอัตราส่วนของเมทานอลเกิดขึ้นมากที่สุด จากนั้นจึงนำตัวเร่งปฏิกิริยาไปทำปฏิกิริยาที่อุณหภูมิ 400 องศาเซลเซียส ความดัน 10 บาร์เป็นระยะเวลา 5 ชั่วโมงเพื่อทำการศึกษาการเสื่อมสมรรถภาพของตัวเร่งปฏิกิริยาต่อไป โดยจากการศึกษาพบว่าตัวเร่งปฏิกิริยาที่สังเคราะห์ขึ้นทุกชนิดมีการเกิดขึ้นของเมทานอลน้อยมากเมื่อเทียบกับคาร์บอนมอนอกไซด์ ดังนั้นจึงเหมาะแก่การใช้ในปฏิกิริยา Reverse water-gas shift (RWGS) มากกว่า

สาขาวิชา      วิศวกรรมเคมี  
ปีการศึกษา    2565

ลายมือชื่อนิสิต .....  
ลายมือชื่อ อ.ที่ปรึกษาหลัก .....

# # 6370302521 : MAJOR CHEMICAL ENGINEERING

KEYWORD: MCF-Si, SBA-15, Cu catalyst, CO<sub>2</sub> hydrogenation, RWGS reaction

Sirimas Suelueam : CHARACTERISTICS AND CATALYTIC PROPERTIES OF COPPER ON MCF-Si AND SBA-15 FOR HYDROGENATION OF CARBON DIOXIDE . Advisor: Prof. BUNJERD JONGSOMJIT, Ph.D.

At present, the production of methanol from the hydrogenation of carbon dioxide is widespread. The current popular catalysts include copper oxide, zinc oxide and aluminum oxide (CZA) catalysts. As the reaction progresses, the catalyst forms coke. This causes the efficiency of the catalyst to decrease. In this study, the copper catalyst on the mesoporous silica support was investigated. This type of support has high thermal stability. Cu catalysts were synthesized on MCF-Si and SBA-15 supports with different pore morphology such as spherical and hexagonal shape, respectively, by wetness impregnation (W) method and incipient wetness impregnation (IW) with a copper loading of 60 wt%. The synthesized catalysts were then subjected to physical and chemical characterization by SEM-EDX, XRF, XRD, TEM, N<sub>2</sub> physisorption, TGA, CO-chemisorption and H<sub>2</sub>-TPR. It was found that metal impregnation of the support in both methods did not change the structural characteristics. Before taking the catalyst to hydrogenation with CO<sub>2</sub> and H<sub>2</sub>, the reaction is divided into 2 parts: the first part was tested at a temperature range of 100-400°C under pressure of 10 bar, to study the optimum temperature for each catalyst. The Cu catalyst supported on MCF-Si had the highest ratio of methanol at 300 °C. However, the catalyst supported by SBA-15 had the highest selectivity of methanol at 400 °C. In the second part, the catalyst was then tested at 400 °C under pressure of 10 bar for 5 hours (time on stream) for further study of catalyst deactivation. It revealed that all synthesized catalysts produced very little methanol as compared to carbon monoxide. Therefore, it is more suitable for use in reverse water-gas shift (RWGS) reaction.

Field of Study: Chemical Engineering

Student's Signature .....

Academic Year: 2022

Advisor's Signature .....

## ACKNOWLEDGEMENTS

I would like to express my sincere thanks to my thesis advisor, Professor Dr. Bunjerd Jongsomjit for his invaluable help and constant encouragement throughout the course of research. I am most grateful for his teaching and advice. I would not have achieved this far and this thesis would not have been complete without all of supports that I have always received from his.

In addition, I am grateful for the thesis committee: Professor Dr. Piyasan Prasertdam (Chairman), Professor Dr. Joongjai Panpranot (Examiner) and Associate Professor Dr. Ekrachan Chaichana (External examiner) for suggestion and all their help.

Additionally, I would like to thank all seniors and friends from Center of Excellence on Catalysis and Catalytic reaction engineering (CECC), Chulalongkorn University with great supports and advice.

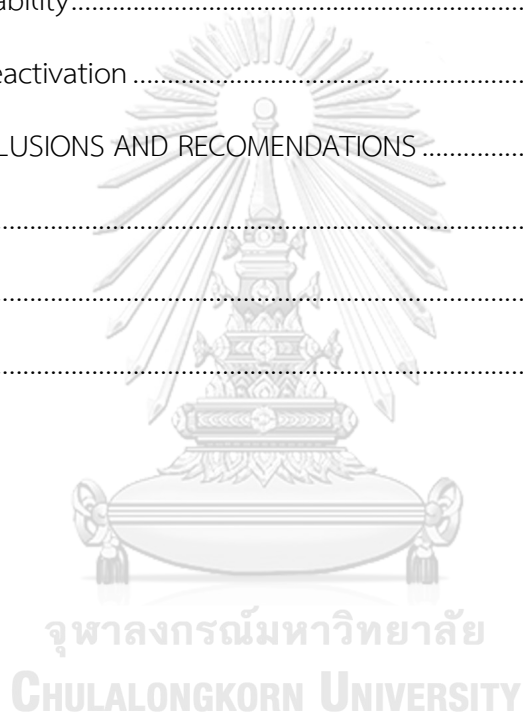
Finally, I most gratefully acknowledge my parents and my friends for all of their support throughout the period of this research.

Sirimas Suelueam

## TABLE OF CONTENTS

	Page
ABSTRACT (THAI) .....	iii
ABSTRACT (ENGLISH) .....	iv
ACKNOWLEDGEMENTS .....	v
TABLE OF CONTENTS .....	vi
LIST OF TABLES .....	viii
LIST OF FIGURES.....	ix
CHAPTER 1 INTRODUCTION.....	1
1.1. Background.....	1
1.2. Research objectives.....	3
1.3. Research scopes.....	3
1.4. Research methodology .....	4
1.5. Research plan .....	6
CHAPTER 2 BACKGROUND AND LITERATURE REVIEW.....	7
2.1. Carbon dioxide.....	7
2.2. Methanol .....	8
2.3. Methanol synthesis via CO <sub>2</sub> hydrogenation.....	8
2.4. Mesoporous materials.....	10
2.5. Cu-based mesoporous catalyst .....	11
2.6. Literature review.....	12
CHAPTER 3 EXPERIMENT .....	40
3.1. Materials .....	40

3.2. Preparation of catalysts .....	40
3.3. Characterization .....	41
3.4. Activity test .....	45
CHAPTER 4 RESULTS AND DISCUSSION .....	48
4.1. Catalysts characterization.....	48
4.2. Screening catalysts.....	61
4.3. Catalysts stability.....	63
4.4. Catalysts deactivation .....	64
CHAPTER 5 CONCLUSIONS AND RECOMENDATIONS .....	66
APPENDIX .....	68
REFERENCES.....	75
VITA .....	81





## LIST OF TABLES

	Page
Table 1. Products obtained by reacting with CO <sub>2</sub> as a precursor .....	1
Table 2. The catalyst and support material of prepared catalysts .....	3
Table 3. Properties of CO <sub>2</sub> .....	7
Table 4. Properties of methanol .....	8
Table 5. The conditions and significant review .....	12
Table 6. The chemical used in catalyst preparation .....	40
Table 7. The operating condition of gas chromatography .....	46
Table 8. The elemental distribution of catalysts .....	51
Table 9. The crystallite size calculated from Scherrer's equation .....	54
Table 10. The BET surface area, pore volume and average pore diameter of catalysts .....	57
Table 11. The surface active site ( $S_{Cu}$ ) and the active sites dispersion (D) .....	59
Table 12. The CO and methanol selectivity of catalysts at 300 and 400 °C .....	62

## LIST OF FIGURES

	Page
Figure 1. The illustration of research methodology .....	5
Figure 2. Molecular structure of carbon dioxide .....	7
Figure 3. Molecular structure of methanol .....	8
Figure 4. Reaction mechanism for methanol synthesis via CO <sub>2</sub> hydrogenation.....	9
Figure 5. Three-dimensional cells and windows in MCF-Si material.....	10
Figure 6. The three-dimensional appearance of the SBA-15 .....	11
Figure 7. The corresponding EDX maps of the combined Cu and Si signal, Cu (red), Si (green), and O (blue) of Cu/MCF-Si.....	11
Figure 8. Experimental set-up for reaction test.....	45
Figure 9. The SEM-EDX images of Cu/MCF-Si (W) catalyst .....	48
Figure 10. The SEM-EDX images of Cu/MCF-Si (IW) catalyst.....	49
Figure 11. The SEM-EDX images of Cu/SBA-15 (W) catalyst .....	49
Figure 12. The SEM-EDX images of Cu/SBA-15 (IW) catalyst.....	50
Figure 13. The low-angle XRD patterns of the MCF-Si supported (above) and the SBA-15 supported (below) catalysts.....	53
Figure 14. The wide-angle XRD patterns of the catalysts .....	54
Figure 15. The TEM micrograph of (a) MCF-Si, (b) Cu/MCF-Si (W) and (c) Cu/MCF-Si (IW) catalysts.....	55
Figure 16. The TEM micrograph of (a) SBA-15, (b) Cu/SBA-15 (W) and (c) Cu/SBA-15 (IW) catalysts .....	56
Figure 17. N <sub>2</sub> physisorption isotherms of MCF-Si and MCF-Si supported catalysts (above) and SBA-15 and SBA-15 supported catalysts (below) .....	58

Figure 18. Temperature programmed reduction (H <sub>2</sub> -TPR) of catalysts.....	60
Figure 19. The CO <sub>2</sub> conversion of catalysts reacted at 100-400 °C.....	62
Figure 20. The CO <sub>2</sub> conversion during time-on-stream of CO <sub>2</sub> hydrogenation for 5 hours at 400 °C. ....	63
Figure 22. The SEM micrograph of (a) Cu/MCF-Si (W), (b) Cu/MCF-Si (IW), (c), Cu/SBA-15 (W) and (d) Cu/SBA-15 (IW).....	64
Figure 23. The temperature programmed profile of spent catalysts after CO <sub>2</sub> hydrogenation for 5 hours at 400 °C.....	64



# CHAPTER 1

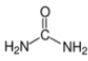
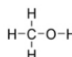
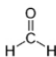
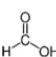
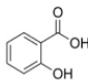
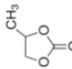
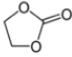
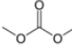
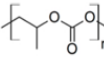
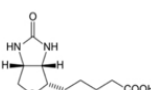
## INTRODUCTION

### 1.1. Background

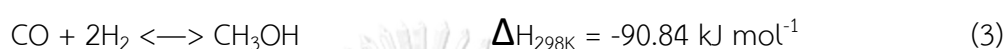
At present, the emission of carbon dioxide from industrial plants continues to be continuously serious problem. Although there are laws that stipulate minimum gas emissions [1], the carbon dioxide emitted still creates problems with global warming. It is interesting to capture the carbon dioxide emitted to convert it into more valuable chemicals.

Carbon dioxide (CO<sub>2</sub>) is a precursor in many reactions and can be processed into a variety of other products as shown in **Table 1**. For example, the production of urea, methanol, formaldehyde, and formic acid etc. [2]. The production of methanol from the hydrogenation of CO<sub>2</sub> with hydrogen is interesting because methanol can be used in many applications. For example, it is used as an organic solvent, fuel, etc.

**Table 1.** Products obtained by reacting with CO<sub>2</sub> as a precursor

Chemical	Molecular Formula	Production (t/year)	CO <sub>2</sub> Consumption (t/year)
Urea		1.5 × 10 <sup>8</sup>	1.12 × 10 <sup>8</sup>
Methanol		1.0 × 10 <sup>8</sup>	2 × 10 <sup>6</sup>
Formaldehyde		9.7 × 10 <sup>6</sup>	
Formic acid		7.0 × 10 <sup>5</sup>	
Salicylic acid		7.0 × 10 <sup>4</sup>	3.0 × 10 <sup>4</sup>
Cyclic carbamate		8.0 × 10 <sup>4</sup>	4.0 × 10 <sup>4</sup>
Ethylene carbamate			
Di-methyl carbamate		1.0 × 10 <sup>7</sup>	
Copolymers			
Polymer-building blocks			
Fine chemical: for example, biotin			

Methanol can be synthesized by hydrogenation of CO<sub>2</sub> via the reaction between carbon dioxide and hydrogen. The product substances are methanol and water. The CO<sub>2</sub> hydrogenation can occur in two pathways [3]: direct CO<sub>2</sub> hydrogenation [Eq.(1)] and reverse water-gas shift (RWGS) [Eq. (2)] continue with CO hydrogenation [Eq. (3)] shown as follows:



Considering the reaction process, it is found that this reaction is exothermic and prefers to occur at high pressure according to Le Chatelier's principle. So, this reaction cannot occur spontaneously. Therefore, a catalyst is used to enable the reaction to proceed.

At present, catalysts are widely invented and developed. Cu-based catalysts have long been used in the hydrogenation of CO and CO<sub>2</sub>. The most commonly used catalysts in this reaction are: copper oxide, zinc oxide and aluminum oxide catalysts (CuO/ZnO/Al<sub>2</sub>O<sub>3</sub>), commonly known as CZA catalyst. However, in the reaction of the CZA catalyst there were still problems. After the reaction, coverage of coke around the active site results in less catalyst stability to catalyze the reaction [4]. Therefore, the development of suitable catalysts is still crucial.

Mesoporous material is a material with suitable properties as catalyst support in various reactions. Due to the uniform porous nature of the material, good pore size distribution, large surface area and a high pore volume, framework/wall substitutions with various metal oxides, biocompatibility and low toxicity [5]. Therefore, the mesoporous materials have many types with different specific pore structure. For instance, MCF-Si is a silica material with a spherical porous structure, whereas SBA-15 is a silica material with a uniform hexagonal porous structure. The difference in the pore structure affects its ability to be supportive.

In this research, the study is divided into 2 consecutive parts. Firstly, the study of Cu-based catalysts on different mesoporous silica supports, MCF-Si and SBA-15, where Cu metal precursor was impregnated onto the supports by the wetness impregnation method (W) and the incipient wetness impregnation method (IW) and then test on the CO<sub>2</sub> hydrogenation reaction at various temperatures, under a pressure of 10 bar. Secondly, a continuation from the first part, the temperature resulting in the catalyst's best efficiency or the highest selectivity of methanol was used to investigate the stability and deactivation of catalysts during CO<sub>2</sub> hydrogenation under time on stream (TOS) compared with commercial CZA catalyst.

### 1.2. Research objectives

To determine the characteristics and catalytic properties of Cu-based catalysts on MCF-Si and SBA-15 prepared by different impregnation methods for CO<sub>2</sub> hydrogenation.

### 1.3. Research scopes

#### 1.3.1. Catalyst preparation

Preparation of Cu-based catalysts on MCF-Si and SBA-15 supports by wetness impregnation (W) and incipient wetness impregnation (IW) methods using 60 wt% of Cu as shown in **Table 2**.

**Table 2.** The catalyst and support material of prepared catalysts

Catalysts	Metal	Support material	Impregnation method	%Cu (wt%)
Cu/MCF-Si (W)	Cu	MCF-Si	Wetness	60
Cu/MCF-Si (IW)	Cu	MCF-Si	Incipient wetness	60
Cu/SBA-15 (W)	Cu	SBA-15	Wetness	60
Cu/SBA-15 (IW)	Cu	SBA-15	Incipient wetness	60

### 1.3.2. Characterization of catalyst

- 1.3.2.1. Scanning electron microscopy (SEM)
- 1.3.2.2. Energy dispersive X-ray spectroscopy (EDX)
- 1.3.2.3. X-ray fluorescence (XRF)
- 1.3.2.4 X-ray diffraction (XRD)
- 1.3.2.5. Transmission electron microscopy (TEM)
- 1.3.2.6. N<sub>2</sub> physisorption
- 1.3.2.7. CO chemisorption
- 1.3.2.8. Temperature-programmed reduction (H<sub>2</sub>-TPR)
- 1.3.2.9. Thermogravimetric analysis (TGA)

### 1.3.3. Activity test

1.3.3.1. Testing the activity of catalysts in CO<sub>2</sub> hydrogenation by temperature-programmed reaction at 100-400 °C under pressure 10 bar with feeding reactants consisting of CO<sub>2</sub>:H<sub>2</sub> = 1:3.

1.3.3.2. Testing the stability and deactivation of the catalyst at the temperature that gives the highest yield of methanol in CO<sub>2</sub> hydrogenation under pressure 10 bar with feeding reactants consisting of CO<sub>2</sub>:H<sub>2</sub> = 1:3 for 5 hours.

## 1.4. Research methodology

Part 1: Catalyst screening: CO<sub>2</sub> hydrogenation using Cu-based catalyst with MCF-Si and SBA-15 supports by temperature-programmed reaction.

Part 2: Stability and deactivation: CO<sub>2</sub> hydrogenation using Cu-based catalyst with MCF-Si and SBA-15 supports at temperatures yielding the highest methanol selectivity from part 1 for 5 hours.

The research methodology is illustrated in **Figure 1**.

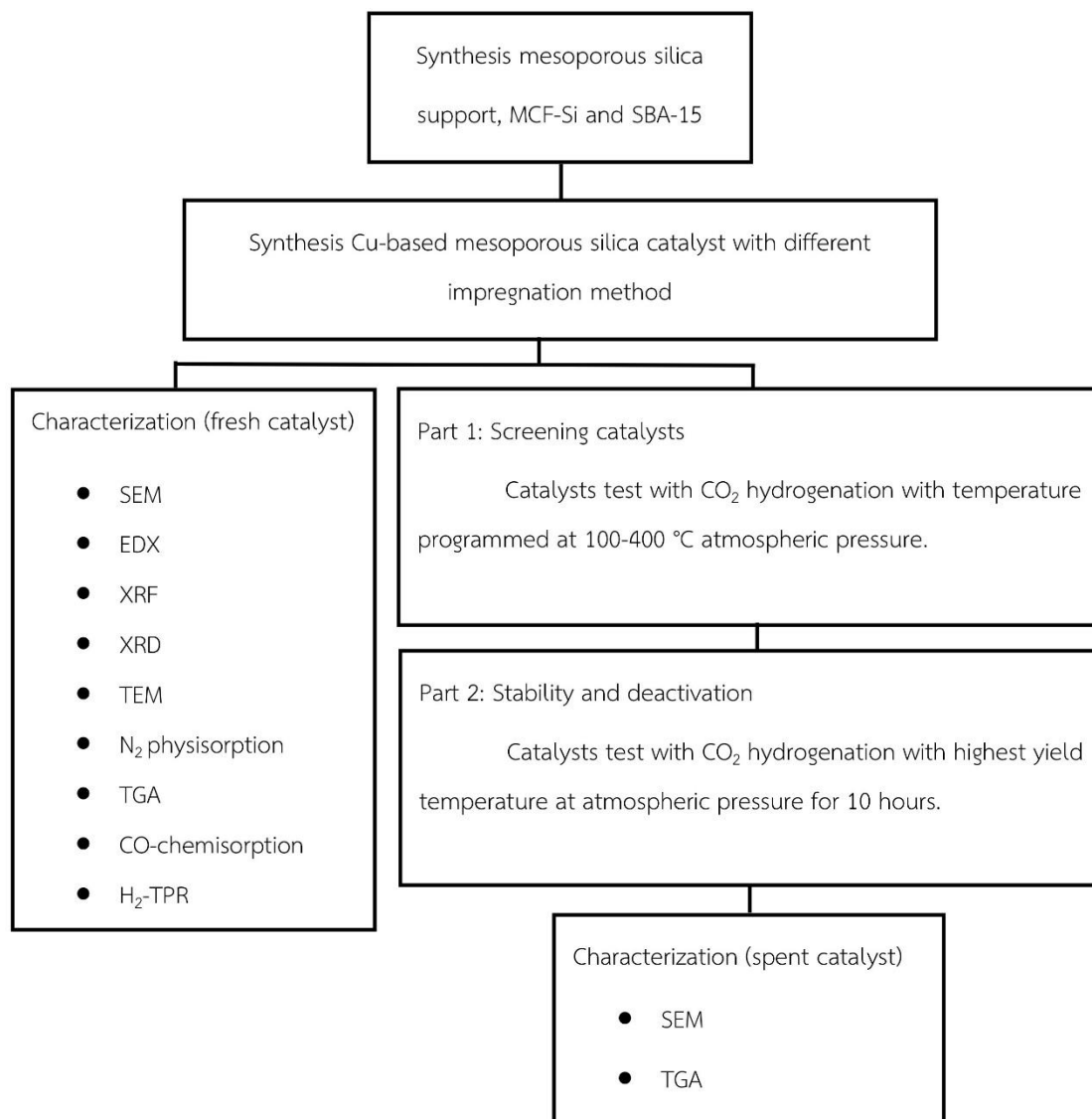


**Figure 1.** The illustration of research methodology



## 1.5. Research plan

Research plan	Semester 2 of 2021			Semester 1 of 2022		
	Jan	Mar	May	Jul	Sep	Nov
1.Literature review	■	■				
2.Preparation of MCF-Si and SBA-15 supports		■	■			
3.Preparation of Cu-based on MCF-Si and SBA-15 with different impregnation method		■	■			
4.Characterization of all catalysts			■	■		
5.Test hydrogenation of CO <sub>2</sub>				■	■	
6.Analysis, Discussion and Conclusion					■	■
7.Thesis writing					■	■

## CHAPTER 2

### BACKGROUND AND LITERATURE REVIEW

#### 2.1. Carbon dioxide

Carbon dioxide (chemical formula: CO<sub>2</sub>) is a molecule composed of two covalent double bonds between one carbon atom and two oxygen atoms shown in **Figure 2**. Under normal conditions, it is a colorless, odorless, non-flammable, weakly acidic gas and soluble in water [6].



**Figure 2.** Molecular structure of carbon dioxide

CO<sub>2</sub> can be used as a reactant in a wide variety of reactions. The properties of CO<sub>2</sub> are shown in **Table 3**. CO<sub>2</sub> is a useful gas. But at present there is a large amount of CO<sub>2</sub> emissions from the industrial sector. This affects the environment, especially the problem of global warming, where CO<sub>2</sub>, which is one of the most common GHGs.

**Table 3.** Properties of CO<sub>2</sub>

Properties	Information
Molecular weight	44.009 g/mol
Density	1.799 g/L
Boiling point	-78.48 °C
Melting point	-56.50 °C
Vapor pressure	5720 kPa at 20°C
Appearance	Colorless gas

## 2.2. Methanol

Methanol or methyl alcohol (chemical formula:  $\text{CH}_3\text{OH}$ ) is an organic compound consisting of a methyl group ( $\text{CH}_3$ ) linked to a hydroxy group ( $\text{OH}$ ), shown in Figure 3. It is a clear, volatile, toxic liquid, commonly used as a fuel solvent.

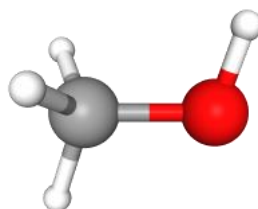


**Figure 3.** Molecular structure of methanol

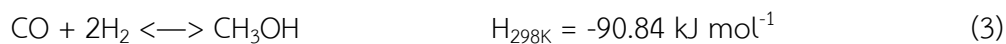
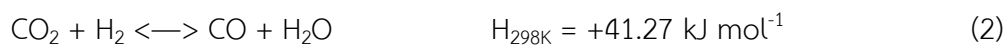
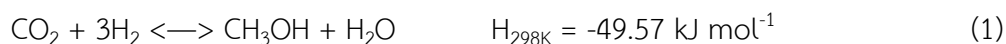
Methanol is used as a precursor to produce most formaldehyde by partial oxidation or use a mixture of gasoline to use as fuel and condensing methanol to obtain hydrocarbon or aromatic compounds. This includes methanol to hydrocarbons (MtH), methanol to gasoline (MtG), methanol to olefins (MtO), and methanol to propylene (MtP). The properties of methanol are shown in **Table 4** [7].

**Table 4.** Properties of methanol

Properties	Information
Molecular weight	32.04 g/mol
Density	0.792 g/L
Boiling point	64.70 °C
Melting point	-97.60 °C
Vapor pressure	13.02 kPa at 20°C
Appearance	Colorless liquid

## 2.3. Methanol synthesis via $\text{CO}_2$ hydrogenation

The  $\text{CO}_2$  hydrogenation can occur in two pathways: direct  $\text{CO}_2$  hydrogenation [Eq.(1)] and reverse water-gas shift (RWGS) [Eq. (2)] continue with CO hydrogenation [Eq. (3)] shown as follows:



Considering the reaction process, it is found that this reaction is exothermic and prefers to occur at high pressure according to Le Chatelier's principle. To make the reaction possible, the reaction must be done at high temperatures which increases the cost. Therefore, a catalyst is used to increase the likelihood of a reaction.

The reactions in each pathways occur as shown in the **figure 4** [2].

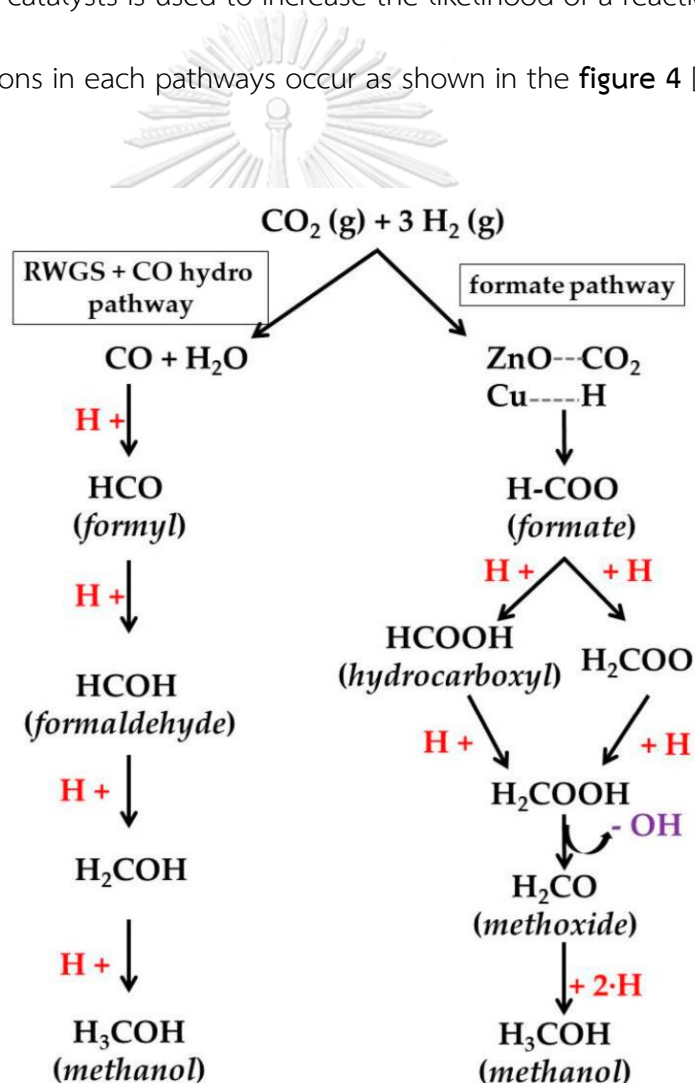


**Figure 4.** Reaction mechanism for methanol synthesis via  $\text{CO}_2$  hydrogenation

## 2.4. Mesoporous materials

Mesoporous material is a porous material of 2–50 nm as defined by the IUPAC, mainly composed of alumina and silica. Important properties of mesoporous materials are narrow pore size distribution and high surface area, structural/surface area replacement with various metal oxides, simple functionalization strategies with organics, biocompatibility and low toxicity. High surface area materials are developed for continuous use as catalysts to decrease energy consumption and industrial waste generation. The choice of mesoporous materials as a catalyst can significantly reduce costs in the industry [8].

### 2.4.1. MCF-Si

Mesostructured cellular foam silica (MCF-Si) is characterized by a porous silica sieve. The spherical shape three-dimensional (3D) arrangement provides thermal stability. MCF silica has pore sizes in the range of 150–500 Å. Their structure consists of spherical cells and windows where the cells (pore sizes: 200–500 Å) are framed by a disordered array of silica struts and the windows (pore sizes: 100–150 Å) interconnect the cells to form a continuous three-dimensional (3D) porous system [9].

The MCF-Si is synthesized in acidic conditions using triblock copolymer Pluronic 123 as a pattern formed by adding a hydrophobic swelling agent such as 1,3,5-trimethylbenzenexylene (TMB) and tetraethoxysilane (TEOS) for the source of silica. Three-dimensional cells and windows in MCF-Si material shown in **Figure 5**.

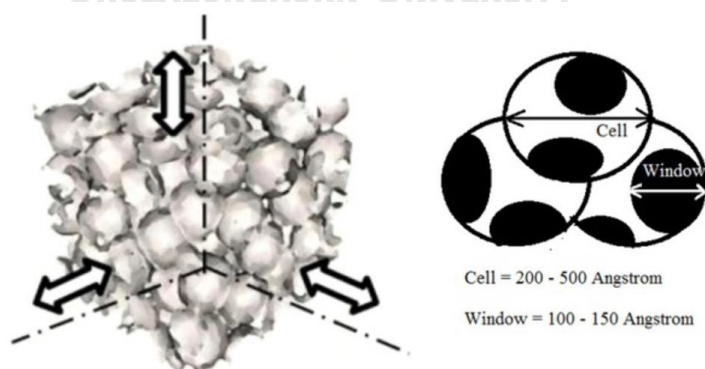


**Figure 5.** Three-dimensional cells and windows in MCF-Si material

### 2.4.2. SBA-15

Santa Barbara Amorphous-15 (SBA-15) is a mesoporous silica sieve with high thermal and mechanical stability. Due to the uniform hexagonal pore structure, 2-dimensional (2D) arrangement and narrow pore size distribution. The pore size is between 5-15 nanometers, thick walls, high internal surface area. It is therefore qualified to be used as a support in a catalyst [10].

Mesoporous silica SBA-15 is synthesized in acidic conditions using triblock copolymer Pluronic 123 as a pattern and tetraethoxysilane (TEOS) for the source of silica. The three-dimensional appearance of the SBA-15 is shown in **Figure 6** [11].

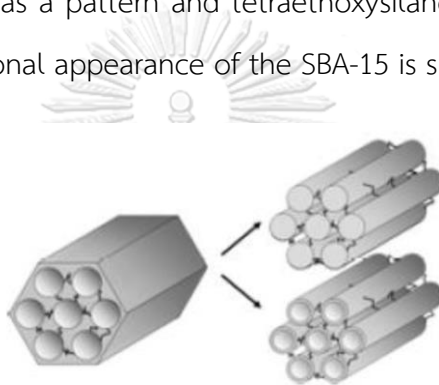


**Figure 6.** The three-dimensional appearance of the SBA-15

### 2.5. Cu-based mesoporous catalyst

Impregnating metals on mesoporous material support can be done in a variety of ways. Different methods affect catalyst efficiency due to the metal distribution. The Cu-containing Cu on MCF-Si shown in **figure 7** [12].

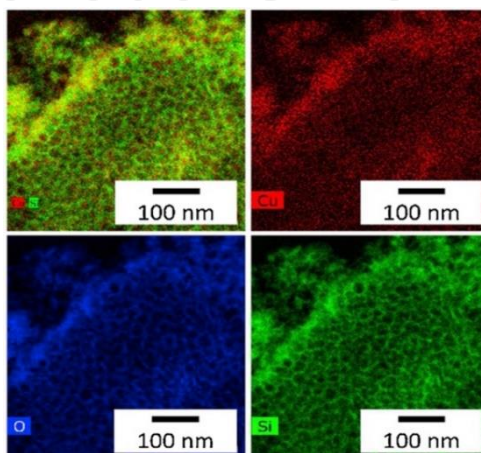


**Figure 7.** The corresponding EDX maps of the combined Cu and Si signal, Cu (red), Si (green), and O (blue) of Cu/MCF-Si

### 2.5.1. Wetness impregnation method (W)

Wetness impregnation method (W), where the precursor and support are dissolved in a solvent before stirring at the appropriate temperature. So that the dissolved metal ions in the solution form new bonds to the desired substance. The solvent is then evaporated and the substance is calcined to make the catalyst ready for use.

### 2.5.2. Incipient wetness impregnation method (IW)

The incipient wetness impregnation (IW), also called capillary impregnation or dry impregnation. A commonly used technique for synthesis of heterogeneous catalysts. The precursor is dissolved in a solvent before it is dripped to the dehydrated support. The solvent is then evaporated and the substance is calcined to make the catalyst ready for use.

## 2.6. Literature review

Research on CO<sub>2</sub> Hydrogenation reactions using mesoporous materials as catalysts, in the scopus database, 2000-2021 shown in **table 5**.

**Table 5.** The conditions and significant review

No.	Published year	Reaction condition	Significant results	Reference
1	2006 (Yu, Y.M.)	<p>Catalysts :</p> <ul style="list-style-type: none"> <li>- Pure MCM-41</li> <li>- MCM-41 functionalized with Y-aminopropyl trimethoxysilane</li> <li>- Functionalized MCM-41 loaded with ruthenium complex</li> </ul> <p>Reactor : Stainless steel autoclave</p> <p>Conditions :</p> <ul style="list-style-type: none"> <li>- CO<sub>2</sub> hydrogenation for the synthesis of formic acid</li> <li>- Total pressure 147 bar</li> <li>- Temperature 80°C</li> <li>- Ratio CO<sub>2</sub>:H<sub>2</sub> = 7:4</li> </ul>	<ul style="list-style-type: none"> <li>- Functionalized MCM-41 and Ru catalyst have lower surface area, pore volume respectively. Meanwhile, the pore diameters of the three catalysts were similar in size.</li> <li>- The use of different solvents and promoters affect the activity of immobilized Ru catalyst.</li> </ul>	[13]



No.	Published year	Reaction condition	Significant results	Reference
2	2006 (Yu, Y.M.)	Reaction condition Catalysts : <ul style="list-style-type: none"> <li>- functionalized MCM-41</li> <li>- M-RuCl<sub>3</sub></li> <li>- M-RuCl<sub>2</sub>(PPh<sub>3</sub>)<sub>3</sub></li> </ul> Reactor Stainless steel autoclave Conditions : <ul style="list-style-type: none"> <li>- Synthesis of formic acid</li> <li>- Temperature 80 °C</li> <li>- Ratio CO<sub>2</sub>:H<sub>2</sub> = 6:4</li> <li>- p<sub>H2</sub> = 50 bar</li> <li>- Ru content = 0.01 mmol</li> <li>- base = 5 mL NEt<sub>3</sub></li> <li>- solvent = 20 mL ethanol</li> <li>- Ligands : Triphenylphosphine</li> </ul>	<ul style="list-style-type: none"> <li>- The catalysts activity increases rapidly with CO<sub>2</sub> pressure to its critical point.</li> <li>- The temperature and pressure influenced the properties of reactant gas and the formation of active species on the catalysts..</li> </ul>	[14]

No.	Published year	Reaction condition	Significant results	Reference
3	2012 (G.G., Morgan)	<p>Catalysts :</p> <ul style="list-style-type: none"> <li>- SBA-15</li> <li>- SBA-15-Cl</li> <li>- SBA-15-Cl-cryptand</li> <li>- Co SBA-15-cryptand</li> <li>- Cu SBA-15-cryptand</li> </ul> <p>Reactor Parr reactor</p> <p>Conditions :</p> <ul style="list-style-type: none"> <li>- Ratio CO<sub>2</sub>:H<sub>2</sub> = 3.05:7.31 mmol</li> <li>- Pressure 45 bar balance with Ar</li> <li>- Temperature 100-200 °C</li> <li>- Time 4 h</li> </ul>	<ul style="list-style-type: none"> <li>- The Cu-containing catalysts produced CH<sub>4</sub> as a primary product whereas the Co-containing catalysts produced both CO and CH<sub>4</sub> as products.</li> <li>- Different temperatures give different CH<sub>4</sub>, CO production and H<sub>2</sub> and CO<sub>2</sub> conversions.</li> </ul>	[15]

No.	Published year	Reaction condition	Significant results	Reference
4	2013 (Zhou., G.)	<p>Catalysts :</p> <ul style="list-style-type: none"> <li>- Co/KIT-6</li> <li>- Co/meso-SiO<sub>2</sub></li> </ul> <p>Reactor : Tubular, continuous-flow, fixed bed quartz reactor</p> <p>Conditions :</p> <ul style="list-style-type: none"> <li>- CO<sub>2</sub> methanation reaction</li> <li>- Atmospheric pressure</li> <li>- Temperature 100-600 °C</li> <li>- Ratio CO<sub>2</sub>:H<sub>2</sub> = 1:4.6 vol% balanced by Ar</li> <li>- The feed gas mixture flow rate 36.67 mL min<sup>-1</sup></li> <li>- Gas mass spece velocity (GMSV) 22,000 mL g<sup>-1</sup> h<sup>-1</sup></li> </ul>	<ul style="list-style-type: none"> <li>- Co/KIT-6 and Co/meso-SiO<sub>2</sub> catalysts have large specific surface areas and high supported Co species dispersion.</li> <li>- The Co/KIT-6 catalyst has a higher CO<sub>2</sub> hydrogenation activity than Co/meso-SiO<sub>2</sub> catalyst</li> </ul>	[16]

No.	Published year	Reaction condition	Significant results	Reference
5	2013 (Kiatphuengporn, S.)	<p>Catalysts :</p> <ul style="list-style-type: none"> <li>- xFe-xCu bimodal and unimodal MCM-41</li> </ul> <p>Reactor Stainless steel tubular reactor</p> <p>Conditions :</p> <ul style="list-style-type: none"> <li>- Pressure 10 bar</li> <li>- Temperature 160-350 °C</li> <li>- Ratio CO<sub>2</sub>:H<sub>2</sub> = 1:3</li> <li>- The gas hourly space velocity (GHSV) 4,800 mL h<sup>-1</sup> g<sub>cat</sub><sup>-1</sup>.</li> </ul>	<ul style="list-style-type: none"> <li>- Both catalytic activities and product selectivities of xFe-10Cu/MCM-41 bimodal and xFe-10Cu/MCM-41 unimodal catalyst for CO<sub>2</sub> hydrogenation reaction were strongly affected by pore characteristics of supports.</li> </ul>	[17]

No.	Published year	Reaction condition	Significant results	Reference
6	2015 (Xiao, J.)	<p>Catalysts :</p> <ul style="list-style-type: none"> <li>- Pd(X)-Cu(Y)/support</li> <li>- Cu-ZnO(Z)/SiO<sub>2</sub></li> </ul> <p>where X, Y and Z represent Pd/(Pd+Cu), Cu/(Pd+Cu) and Zn/(Zn+Cu) and supports are SiO<sub>2</sub>, SBA-15 and MCM-41</p> <p>Reactor : Fixed-bed reactor</p> <p>Conditions :</p> <ul style="list-style-type: none"> <li>- Pressure 41 bar</li> <li>- Temperature 300 °C</li> <li>- The gas hourly space velocity (GHSV) 3,600 mL g cat<sup>-1</sup> h<sup>-1</sup></li> <li>- Time 2 h</li> </ul>	<ul style="list-style-type: none"> <li>- The combination of Cu and Pd led to strong synergistic promotion of CH<sub>3</sub>OH formation rate.</li> <li>- CO<sub>2</sub> appears to be a primary carbon source for methanol formation over Pd-Cu/SiO<sub>2</sub> catalysts at lower CO<sub>2</sub> conversion; while byproduct CO contributes also methanol synthesis through CO hydrogenation at higher CO<sub>2</sub> conversion.</li> </ul>	[18]

No.	Published year	Reaction condition	Significant results	Reference
7	2015 (T, Wilton.)	<p>Catalysts :</p> <ul style="list-style-type: none"> <li>- Cu-loaded unimodal alumina (Cu/UAI)</li> <li>- Cu-loaded hierarchical meso-macroporous alumina (Cu/HAI)</li> </ul> <p>Reactor Fixed-bed stainless steel reactor</p> <p>Conditions :</p> <ul style="list-style-type: none"> <li>- Pressure 30 bar</li> <li>- Temperature 240, 260, 280, 300 and 320 °C</li> <li>- Ratio CO<sub>2</sub>:H<sub>2</sub> = 1:3</li> </ul>	<ul style="list-style-type: none"> <li>- Cu-loaded hierarchical meso-macroporous alumina catalyst (Cu/HAI) exhibited the higher methanol selectivity and stability than Cu-loaded unimodal mesoporous alumina catalyst (Cu/UAI)</li> <li>- Cu/UAI has higher surface area and pore volume than Cu/HAI</li> </ul>	[19]

No.	Published year	Reaction condition	Significant results	Reference
8	2015 (R, Merkache I.)	Catalysts : - Fe-KIT-6 Reactor - Tubular, continuous-flow, fixed-bed quartz reactor Conditions : - Atmospheric pressure - Temperature 250-500 °C - Ratio CO <sub>2</sub> :H <sub>2</sub> = 1:4 balance with N <sub>2</sub>	<ul style="list-style-type: none"> <li>- The catalytic activity of the Fe-KIT-6 catalysts increases significantly with increasing iron content.</li> <li>- The rate of CO<sub>2</sub> hydrogenation on the Fe-KIT-6 catalysts is a function of the iron active site density and the temperature.</li> </ul>	[20]

No.	Published year	Reaction condition	Significant results	Reference
9	2014 (NOOR, A.M.Z.)	<p>Catalysts :</p> <ul style="list-style-type: none"> <li>- SBA-15</li> <li>- Cu/ZnO/SBA-15</li> <li>- Nb/Cu/ZnO/SBA-15</li> </ul> <p>Reactor micro-activity fixed bed reactor</p> <p>Conditions :</p> <ul style="list-style-type: none"> <li>- Pressure 22.5 bar</li> <li>- Temperature 250 °C</li> <li>- Ratio CO<sub>2</sub>:H<sub>2</sub> = 1:3</li> <li>- Time 4 h.</li> </ul>	<ul style="list-style-type: none"> <li>- Nb/Cu/ZnO/SBA-15 has lower surface area and pore volume than Cu/ZnO/SBA-15, but higher pore diameter.</li> <li>- Nb-promoted catalyst gives higher Cu metal area, Cu dispersion, CO<sub>2</sub> conversion, and methanol yield.</li> </ul>	[21]



No.	Published year	Reaction condition	Significant results	Reference
10	2016 (Liu, X.)	<p>Catalysts :</p> <ul style="list-style-type: none"> <li>- Supported molybdenum carbide (<math>y\text{Mo}_2\text{C}/\text{M41}</math>)</li> <li>- Cu-promoted molybdenum carbide using a mechanical mixing method (<math>x\text{Cu}y\text{Mo}_2\text{C}/\text{M41-M}</math>)</li> <li>- Cu-promoted molybdenum carbide using a co-impregnation method (<math>x\text{Cu}y\text{Mo}_2\text{C}/\text{M41-I}</math>)</li> </ul> <p>Reactor</p> <ul style="list-style-type: none"> <li>- High-pressure fixed-bed reactor</li> </ul> <p>Conditions :</p> <ul style="list-style-type: none"> <li>- Pressure 30 bar</li> <li>- Temperature 220 °C</li> <li>- Ratio <math>\text{CO}_2:\text{H}_2 = 1:3</math> balance with Ar</li> <li>- The gas hourly space velocity</li> </ul>	<ul style="list-style-type: none"> <li>- The adsorption and activation of hydrogen primarily occurred on Cu sites, and the adsorption of <math>\text{CO}_2</math> occurred over <math>\text{Mo}_2\text{C}</math> sites.</li> <li>- <math>20\text{Cu}20\text{Mo}_2\text{C}/\text{M41-M}</math> and <math>20\text{Cu}20\text{Mo}_2\text{C}/\text{M41-I}</math> catalysts exhibited significantly increased <math>\text{CH}_3\text{OH}</math> selectivity because the Cu promoter was highly dispersed on the surface of the catalysts.</li> </ul>	[22]

No.	Published year	Reaction condition	Significant results	Reference
11	2017 (A, Atakan.)	Catalysts : - SBA-15 (S) - Zr-SBA-15 (Z) - Cu-(S) - Cu-(Z) Reactor - HPHT cell Conditions : - Pressure 33 bar - Temperature 250 °C - Ratio CO <sub>2</sub> :H <sub>2</sub> = 1:3 - Time 2 h.	- Cu-(Z) gives higher % conversion of DME and methanol than Cu-(S).	[23]

No.	Published year	Reaction condition	Significant results	Reference
12	2016 (Kiatpungporn, S.)	<p>Catalysts :</p> <ul style="list-style-type: none"> <li>- w(Fe)-w(Cu)/MCM-41 with magnetic flux density</li> </ul> <p>Reactor</p> <p>Magnetic field-assisted, continuous-flow packed-bed reactor</p> <p>Conditions :</p> <ul style="list-style-type: none"> <li>- Pressure 10 bar</li> <li>- Temperature 180-260 °C</li> <li>- Time-on-steam 1 h per each reaction temperature.</li> </ul>	<ul style="list-style-type: none"> <li>- CO<sub>2</sub> conversion and methanol production of all catalysts were significantly improved with the external magnetic field.</li> <li>- The application of magnetic field led to the advantages in a heterogeneously catalyzed reaction as it promoted CO<sub>2</sub> adsorption ability and methanol production.</li> </ul>	[24]

No.	Published year	Reaction condition	Significant results	Reference
13	2016 (Kruatim, J.)	Catalysts : - Co/SBA-15 - Co/SBA-16 with ultrasound and vacuum treatment Reactor Fixed-bed microreactor Conditions : - Atmospheric pressure - Temperature 220 °C - Ratio CO <sub>2</sub> :H <sub>2</sub> = 1:10	<ul style="list-style-type: none"> <li>- The vacuum and ultrasound treatment after impregnation were employed for the Co/SBA-15 and Co/SBA-16.</li> <li>- Both treatments can enhance the cobalt dispersion of the cobalt metal on the SBA-15. However, only vacuum treatment was suitable for improving the cobalt dispersion on the Co/SBA-16.</li> </ul>	[25]

No.	Published year	Reaction condition	Significant results	Reference
14	2017 (Liu, Q.)	<p>Catalysts :</p> <ul style="list-style-type: none"> <li>- NiO/SBA-15 monolith compared to the impregnation (Im) and one-pot method (Op)</li> </ul> <p>Conditions :</p> <ul style="list-style-type: none"> <li>- Atmospheric pressure</li> <li>- Temperature 300-550 °C</li> <li>- The gas hourly space velocity (GHSV) 10,000 mL g cat<sup>-1</sup> h<sup>-1</sup></li> </ul>	<ul style="list-style-type: none"> <li>- The one-pot prepared NiO/SBA-15-Op exhibited much high surface area, large pore volume and high Ni dispersion compared to NiO/SBA-15-Im synthesized.</li> <li>- NiO/SBA-15-Op shown higher activity and stability than NiO/SBA-15-Im because of the high Ni dispersion and more Ni particles dispersed in the meso-channels.</li> </ul>	[26]

No.	Published year	Reaction condition	Significant results	Reference
15	2012 (G.G., Morgan)	<p>Catalysts :</p> <ul style="list-style-type: none"> <li>- Zeolite-based catalysts               <ul style="list-style-type: none"> <li>○ 15%Ni/HNaUSY</li> <li>○ 7%Ce15%Ni/HNaUSY</li> </ul> </li> <li>- SBA-15 based catalysts               <ul style="list-style-type: none"> <li>○ 15%Ni/SBA-15 CL</li> <li>○ 15%Ce15%Ni/SBA-15 CL</li> <li>○ 15%Ni/SBA-15 MW</li> <li>○ 15%Ce15%Ni/SBA-15 MW</li> </ul> </li> <li>- MCM-41 based catalysts               <ul style="list-style-type: none"> <li>○ 15%Ni/MCM-41</li> <li>○ 15%Ce15%MCM-15</li> </ul> </li> </ul> <p>Conditions :</p> <ul style="list-style-type: none"> <li>- Atmospheric pressure</li> <li>- Temperature 250-450 °C</li> <li>- Molar ratio CO<sub>2</sub>:H<sub>2</sub>:N<sub>2</sub> = 36:9:10</li> <li>- The gas hourly space velocity (GHSV) 43,000 and 15,000 mL g cat<sup>-1</sup> h<sup>-1</sup></li> </ul>	<ul style="list-style-type: none"> <li>- SBA-15 based catalysts have higher surface area, external surface area than MCM-41 and HNaUSY respectively.</li> <li>- NiO particle sizes affected by the support type since materials with bigger pore (e.g. SBA-15) could accommodate metal oxides allowing better metal dispersions on the catalysts surface.</li> </ul>	[27]

No.	Published year	Reaction condition	Significant results	Reference
16	2018 (Gao, X.)	<p>Catalysts :</p> <ul style="list-style-type: none"> <li>- Ni/ZSM-5</li> <li>- Ni-SBA-15</li> <li>- Ni/MCM-41</li> <li>- Ni/Al<sub>2</sub>O<sub>3</sub></li> <li>- Ni/SiO<sub>2</sub></li> </ul> <p>Reactor Fixed-bed quartz reactor</p> <p>Conditions :</p> <ul style="list-style-type: none"> <li>- Atmospheric pressure</li> <li>- Temperature 200-450 °C</li> <li>- Ratio CO<sub>2</sub>:H<sub>2</sub> = 1:4</li> <li>- The gas hourly space velocity (GHSV) 2,400 mL g cat<sup>-1</sup> h<sup>-1</sup></li> </ul>	<ul style="list-style-type: none"> <li>- The Ni/ZSM-5 catalyst exhibited the highest CO<sub>2</sub> conversion among all the samples with 99% CH<sub>4</sub> selectivity.</li> <li>- The Ni/ZSM-5 catalyst maintain good stability with no deactivation during the entire experiment period.</li> </ul>	[28]

No.	Published year	Reaction condition	Significant results	Reference
17	2018 (Liu, H.)	Catalysts : - Co/KIT-6 with different Co loading (15-30 wt%) Reactor Micro fixed-bed reactor Conditions : - Atmospheric pressure - Temperature 240-400 °C - Ratio CO <sub>2</sub> :H <sub>2</sub> = 1:4 balance with Ar - The gas hourly space velocity (GHSV) 60,000 mL g cat <sup>-1</sup> h <sup>-1</sup>	<ul style="list-style-type: none"> <li>- The Co/KIT-6 with Co loading 25% has enough highly dispersed metal Co species, superior CO<sub>2</sub> and/or H<sub>2</sub> adsorption abilities.</li> <li>- The Co/KIT-6 with Co loading 25% has highest reaction rate and CH<sub>4</sub> selectivity at 360 °C.</li> <li>- The good dispersion and suitable crystal size of metal Co in the Co/KIT-6 with Co loading 25% catalyst constitute its potential to be an excellence catalyst on CO<sub>2</sub> hydrogenation reaction.</li> </ul>	[29]



No.	Published year	Reaction condition	Significant results	Reference
18	2018 (A, Atakan.)	Catalysts : - Cu-Zr-SBA-15 Reactor Batch reactor Conditions : - Pressure 33 bar - Temperature 250 °C - Ratio CO <sub>2</sub> :H <sub>2</sub> = 1: 3	<ul style="list-style-type: none"> <li>- With higher Zr content in the catalyst, greater selectivity for methanol.</li> <li>- Both DME and methanol selective systems show the thermodynamically highest possible conversion.</li> </ul>	[30]

No.	Published year	Reaction condition	Significant results	Reference
19	2018 (Wang, X.)	<p>Catalysts :</p> <ul style="list-style-type: none"> <li>- Ni/MCM-41 promoted with CeO<sub>2</sub></li> </ul> <p>Reactor</p> <p>Stainless steel tube reactor</p> <p>Conditions :</p> <ul style="list-style-type: none"> <li>- Atmospheric pressure</li> <li>- Temperature 240-500 °C</li> <li>- Ratio CO<sub>2</sub>:H<sub>2</sub> = 1: 4</li> </ul>	<ul style="list-style-type: none"> <li>- The dispersion of Ni on the catalysts was affected by the structure of the support, and the CeO<sub>2</sub> promoted catalysts could stabilize the nickel species more effectively.</li> </ul>	[31]

No.	Published year	Reaction condition	Significant results	Reference
20	2018 (N.H., Berahim.)	<p>Catalysts :</p> <ul style="list-style-type: none"> <li>- SBA-15</li> <li>- Cu/ZnO/Fe/K/Rh/SBA-15</li> <li>- Cu/Al/Fe/K/Rh/SBA-15</li> </ul> <p>Reactor Micro-activity fixed-bed reactor</p> <p>Conditions :</p> <ul style="list-style-type: none"> <li>- Pressure 30 bar</li> <li>- Temperature 250 °C</li> <li>- Ratio CO<sub>2</sub>:H<sub>2</sub> = 1:3</li> <li>- The gas hourly space velocity (GHSV) 5,760 mL g cat<sup>-1</sup> h<sup>-1</sup></li> </ul>	<ul style="list-style-type: none"> <li>- The loaded metal catalyst to the bare support resulted in a decrease of the BET surface area.</li> <li>- Hybrid Cu/Al/Fe/K/Rh/SBA-15 catalyst exhibited higher activity in terms of CO<sub>2</sub> conversion as compared of Cu/ZnO/Fe/K/Rh/SBA-15 catalyst.</li> </ul>	[32]

No.	Published year	Reaction condition	Significant results	Reference
21	2019 (A, Atakan.)	Catalysts : - Cu/Zr/SBA-15 synthesized using two different silica precursors, TEOS and SMS and was loading Cu using two difference impregnation method, infiltration (Inf) and evaporation induced wetness impregnation (EIWI) Reactor High pressure high temperature (HPHT) cell Conditions : - Pressure 33 bar - Temperature 250 °C - Ratio CO <sub>2</sub> :H <sub>2</sub> = 1 : 3	- TEOS yielded materials with larger pores and specific surface area as well as increased microporosity compared to SMS. - Supports synthesized with the Inf method yielded DME and methanol with higher selectivity for DME. - Supports synthesized with the EIWI method yielded DME and methanol with higher selectivity for DME. - Supports synthesized with the EIWI method yielded DME and methanol because their surface acid sites had different strength..	[33]

No.	Published year	Reaction condition	Significant results	Reference
22	2019 (M, Mureddu.)	Catalysts : - CuO/ZnO/ZrO <sub>2</sub> @SBA-15 Reactor High-pressure fixed bed stainless steel reactor Conditions : - Pressure 33 bar - Temperature 250 °C - Ratio CO <sub>2</sub> :H <sub>2</sub> = 22.5:67.5 balance with N <sub>2</sub> - Time 2 h.	- The methanol yield and methanol selectivity are strongly influenced by: (i) The active phase loading and the copper/zinc molar ratio leading to differences in the morphology and dispersion of the active phase. (ii) The presence of zirconia enhances both the yield and selectivity of methanol.	[34]

No.	Published year	Reaction condition	Significant results	Reference
23	2020 (Cao, H.)	<p>Catalysts :</p> <ul style="list-style-type: none"> <li>- 10Ni/KIT-6</li> <li>- 10Ni-0.5V/KIT-6</li> <li>- 20Ni-0.5V/KIT-6</li> </ul> <p>Reactor Continuous flow fixed-bed reactor</p> <p>Conditions :</p> <ul style="list-style-type: none"> <li>- Atmospheric pressure</li> <li>- Temperature 550 °C</li> <li>- Ratio CO<sub>2</sub>:H<sub>2</sub>:N<sub>2</sub> = 1:4:3</li> <li>- The gas hourly space velocity (GHSV) 96,000 mL g cat<sup>-1</sup> h<sup>-1</sup></li> </ul>	<ul style="list-style-type: none"> <li>- 20Ni-0.5V/KIT-6 demonstrate the best reducibility and Ni dispersion.</li> <li>- The synergistic effect between Ni and V could strengthen surface basicity to elevate the ability of CO<sub>2</sub> activity on the 20Ni-0.5V/KIT-6.</li> </ul>	[35]

No.	Published year	Reaction condition	Significant results	Reference
24	2020 (S, Gupta.)	<p>Catalysts :</p> <ul style="list-style-type: none"> <li>- <math>\text{Co}_3\text{O}_4</math>-nano</li> <li>- m-Co-SBA-15</li> <li>- m-Co-KIT-6</li> </ul> <p>Reactor Plug-flow tubular quartz reactor</p> <p>Conditions :</p> <ul style="list-style-type: none"> <li>- Atmospheric pressure</li> <li>- Temperature 280-400 °C</li> <li>- Ratio <math>\text{CO}_2:\text{H}_2:\text{N}_2 = 1:3:0.5</math></li> <li>- The gas hourly space velocity (GHSV) 10,800 <math>\text{mL g cat}^{-1} \text{h}^{-1}</math></li> </ul>	<p>The order of <math>\text{CO}_2</math> hydrogenation activity is m-Co-KIT-6 &gt; m-Co-SBA-15 &gt; nano-<math>\text{Co}_3\text{O}_4</math>.</p>	[36]

No.	Published year	Reaction condition	Significant results	Reference
25	2020 (M.A., Paviotti.)	<p>Catalysts :</p> <ul style="list-style-type: none"> <li>- MCM-41</li> <li>- MCF_ch</li> <li>- MCF_hcp</li> <li>- MCF pvp</li> </ul> <p>Conditions :</p> <ul style="list-style-type: none"> <li>- Atmospheric pressure</li> <li>- Temperature 200-400 °C</li> <li>- Ratio CO<sub>2</sub>:H<sub>2</sub> = 1:4</li> <li>- The gas hourly space velocity (GHSV) 8,600 mL g cat<sup>-1</sup> h<sup>-1</sup></li> </ul>	<ul style="list-style-type: none"> <li>- The best performance of Ni/MCF_ch_iwi could be related to the homogeneous distribution of Ni nanoparticles and to the 3D open structure of the MCF_ch support.</li> <li>- Ni/MCF_ch_iwi showed high structure and catalytic stability, as well as high coke resistance.</li> </ul>	[37]



No.	Published year	Reaction condition	Significant results	Reference
26	2021 (P, Hongmanorom )	<p>Catalysts :</p> <ul style="list-style-type: none"> <li>- Ni-Mg/SBA-15</li> </ul> <p>Reactor</p> <p>Fixed-bed quartz reactor</p> <p>Conditions :</p> <ul style="list-style-type: none"> <li>- Atmospheric pressure</li> <li>- Temperature 200-400 °C</li> <li>- Ratio CO<sub>2</sub>:H<sub>2</sub> = 1:4</li> <li>- The gas hourly space velocity (GHSV) 30,000 mL g cat<sup>-1</sup> h<sup>-1</sup></li> </ul>	<ul style="list-style-type: none"> <li>- The promoted Mg showed medium basic sites that correlated with the TOF and CO<sub>2</sub> conversion.</li> <li>- Ni and Ni-Mg-phyllsilicate structure derived catalysts shown better catalytic stability by suppressing metal sintering through strong metal-support interaction and confinement effect of SBA-15.</li> </ul>	[38]

No.	Published year	Reaction condition	Significant results	Reference
27	2022 (C, Sun.)	<p>Catalysts :</p> <ul style="list-style-type: none"> <li>- Ni-Ce-Y/SBA-15</li> </ul> <p>Reactor</p> <p>U-type tubular quartz reactor</p> <p>Conditions :</p> <ul style="list-style-type: none"> <li>- Atmospheric pressure</li> <li>- Temperature 550 °C</li> <li>- Ratio CO<sub>2</sub>:H<sub>2</sub>:Ar = 15:60:25</li> <li>- The gas hourly space velocity (GHSV) 12,000 mL g cat<sup>-1</sup> h<sup>-1</sup></li> <li>- Time 1.5 h.</li> </ul>	<ul style="list-style-type: none"> <li>- Yttrium as a promoter contributed to an increase of Ce<sup>3+</sup> ratio and number of medium basic sites and enhanced the reducibility of Ni species.</li> <li>- Both catalysts 15Ni10Ce/SBA-15 and 15Ni10Ce10Y/SBA-15 revealed stable CO<sub>2</sub> conversions without any activity loss during a 7 h of time-on-steam experiment at 350 °C.</li> </ul>	[39]

## CHAPTER 3

### EXPERIMENT

#### 3.1. Materials

A list of chemicals that were used in the catalyst preparation is shown in **table 6.**

**Table 6.** The chemical used in catalyst preparation

Chemicals	Formula	Grade	Supplier
Copper (II) nitrate trihydrate	$\text{Cu}(\text{NO}_3)_2 \cdot 3\text{H}_2\text{O}$	98%	Sigma-Aldrich
Pluronic P-123	PEG-PPG-PEG	-	Sigma-Aldrich
Tetraethyl orthosilicate (TEOS)	$\text{Si}(\text{OC}_2\text{H}_5)_4$	98%	Sigma-Aldrich
Mesitylene (TMB)	$\text{C}_6\text{H}_3(\text{CH}_3)_3$	98%	Sigma-Aldrich

The catalyst used for comparison was a CZA catalyst produced by Alfa Aesar. The catalyst consisted of CuO, ZnO, Al<sub>2</sub>O<sub>3</sub> and MgO in ratios of 60-68, 22-26, 8-12 and 1-3 % respectively. The catalyst has a pellets form, dark brown to black appearance, particle size 5.4 nm x 3.6 nm and insoluble in water.

#### 3.2. Preparation of catalysts

##### 3.2.1. mesoporous support

##### 3.2.1.1. MCF-Si

The MCF-Si support was synthesized by mixing 2 g of Pluronic P-123 with a hydrochloric solution and stirred until homogeneous, then add 7 g of TMB and keep stirring and raised temperature to 40°C, then continued stirring for 2 hours. Secondly, slowly drop 4 g of TEOS solution while stirring at 40 °C for 5 min. Next, the solution is placed in a sealed container. It was then heated at 40 °C for 20 hours, followed by at 100°C for another 24 hours. The resulting solution was filtered and washed with ethanol and DI water until the pH neutral. Finally, the white powder was dried at room temperature overnight.

### 3.2.1.2. SBA-15

The SBA-15 support was synthesized by mixing 2 g of Pluronic P-123 with a hydrochloric solution and stirred until homogeneous, then continued stirring for 2 hours. Secondly, slowly drop 4 g of TEOS solution while stirring at 40 °C for 5 min. Next, the solution is placed in a sealed container. It was then heated at 40 °C for 20 hours, followed by at 100°C for another 24 hours. The resulting solution was filtered and washed with ethanol and DI water until the pH neutral. Finally, the white powder was dried at room temperature overnight.

### 3.2.2. Cu impregnation

#### 3.2.2.1. Wetness impregnation method

First, 1 g of support was dissolved in 17 ml of DI water, stirred for 30 min, and then 5.7 g  $\text{Cu}(\text{NO}_3) \cdot 3\text{H}_2\text{O}$  was dissolved in 3 ml of water until homogeneous. Slowly drop the copper solution into the support solution. Raise the temperature to 60°C and continue stirring for 1 hour. The resulting solution was dehydrated at 110°C overnight and calcined at 500°C for 5 hours.

#### 3.2.2.2. Incipient wetness impregnation method

Use 0.1 g of the support to test the weight of the water dampening the support to calculate the weight of water required per 1 g of support. Then, after the water weight is obtained, weighed 5.7 g of  $\text{Cu}(\text{NO}_3) \cdot 3\text{H}_2\text{O}$  and dissolved in the previously calculated DI water. Then, slowly dropped onto 1 g of support and mixed until homogeneous and dehydrated at 110°C overnight and it was calcined at 500°C for 5 hours.

### 3.3. Characterization

#### 3.3.1. Scanning electron microscopy (SEM)

Scanning electron microscopy (SEM) observation with JOEL mode JSM-6400 was used to investigate the morphology of catalysts.

### 3.3.2. Energy dispersive X-ray spectroscopy (EDX)

Energy dispersive X-ray spectroscopy (EDX) using Link Isis series 300 program was used to investigate elemental dispersion on surface of catalysts.

### 3.3.3. X-ray fluorescence spectrometer (XRF)

X-ray fluorescence spectrometer (XRF) used PANalytical MiniPal 4 EDXRF spectrometer equipped with a 30 kV rhodium anode tube with a helium purge facility. The detector was used to count X-rays intensity. XRF was used to investigate the total elemental in the catalysts.

### 3.3.4. X-ray diffraction (XRD)

X-ray diffraction (XRD) patterns were recorded on BRUKER model D8 Advance in the range  $0.5^\circ < 2\theta < 5^\circ$  and Bruker AXS Model D8 with Cu-K $\alpha$  radiation ( $\gamma = 0.154439$  nm) in the range  $10^\circ < 2\theta < 80^\circ$  to analyze crystal structure and crystallite size by Scherrer equation as follows:

$$D = \frac{K\gamma}{\beta \cos\theta}$$

Where:  $D$  = volume average crystallite size

$K$  = unity constant factor

$\gamma$  = X-ray wavelength

$\theta$  = the position of observe peak

$\beta$  = X-ray diffraction broadening in half peak

### 3.3.5. Transmission electron microscopy (TEM)

Transmission electron microscopy (TEM) observation with JEOL JEM-2010 microscopy was used to investigate microstructure. The catalysts were prepared on the Cu grid by dispersing the catalysts in the liquid medium. The samples were then shaken with sonication for about 15 minutes, before dropping the samples onto the grid and letting it dry.

### 3.3.6. N<sub>2</sub> physisorption

N<sub>2</sub> physisorption was used to investigate the surface area by Brunauer-Emmett-Teller (BET) analysis. Also, the method of Barrett-Joyner-Halenda (BJH) was used to investigate average pore size and pore volume. The determination of N<sub>2</sub> gas adsorption at liquid nitrogen temperature (-196°C) in the automation of Micromeritics ASAP 2000.

### 3.3.8. CO-chemisorption

The number of surface active sites and active site dispersion were determined by CO-chemisorption. In the first step, 0.05 g of catalyst was reduced by H<sub>2</sub> gas at 300°C for 1 hour to convert CuO to Cu<sup>0</sup>. Then passing He gas at 25 mL/min for 30 minutes was performed. The catalyst was cooled down to 30 °C. Next, 80 μL CO gas was injected until the catalyst was saturated, which can be calculated the number of active size and active site dispersion by:

$$MSA_s = S_f \times \frac{V_{ads}}{V_g} \times \frac{100\%}{\%M} \times N_A \times \sigma_m \times \frac{m^2}{10^{18}nm^2}$$

Where  $MSA_s$  = surface-active sites

$S_f$  = stoichiometry factor

$V_{ads}$  = volume adsorbed, (cm<sup>3</sup>/g)

$V_g$  = molar volume of gas at STP, 22414 (cm<sup>3</sup>/mol)

$N_A$  = Avogadro's number, 6.023x10<sup>23</sup> (molecules/mol)

$\sigma_m$  = cross-sectional area of active metal atom, (nm<sup>2</sup>)

$$D(\%) = S_f \times \frac{V_{ads}}{V_g} \times \frac{m.w.}{\%M} \times 100\%100\%$$

Where ***D***(%) = active site dispersion

***S<sub>f</sub>*** = stoichiometry factor

***V<sub>ads</sub>*** = volume adsorbed, (cm<sup>3</sup>/g)

***V<sub>g</sub>*** = molar volume of gas at STP, 22414 (cm<sup>3</sup>/mol)

m.w. = molecular weight of the metal, (a.m.u.)

%M = %metal, (%)

### 3.3.9. Temperature-programmed reduction (TPR)

The reduction behavior of catalysts was investigated by temperature-programmed reduction (TPR). In the first step, 0.05 g of sample was pretreated by passing N<sub>2</sub> gas at 300 °C for 1 hour, and then cooled down to ambient temperature. TPR analysis was performed from 25 to 500 °C under the flow of 10% H<sub>2</sub>/Ar with a ramping rate of 10 °C/min.

### 3.3.9. Thermogravimetric analysis (TGA)

The decomposition of spent catalyst was determined by thermogravimetric analysis (TGA). The catalyst sample of 0.02 g was analyzed by using TA Instruments SDT Q 600 analyzer with temperature ramp from 25-1000°C and heating rate 10°C/min under flowing of air 400 ml/min.

### 3.4. Activity test

#### Part 1: Screening of catalysts

CO<sub>2</sub> hydrogenation was performed in micro packed bed reactor. The reaction system is shown in **Figure 8**. First, 0.1 g of catalyst and 0.05 g of quartz wool were packed into the packed-bed continuous flow microreactor (O.D. 1.2 cm, I.D. 1.0 cm, height 50 cm), the catalyst was pretreated to remove moisture and impurities at flowing N<sub>2</sub> at 250°C for 30 min. Next, flow H<sub>2</sub> (40 ml/min) at 300°C for 1 hour to transform Cu oxides in catalysts into Cu<sup>0</sup> metal with reduction. Then, CO<sub>2</sub> hydrogenation was performed [gas hourly space velocity (GHSV) = 24,000 ml/g<sub>cat</sub>h] with temperature program from 100-400°C under pressure 10 bar and volumetric ratio of CO<sub>2</sub>:H<sub>2</sub> is 1:3 balance with N<sub>2</sub>. The reaction products were also analyzed for every 100°C of increased temperature by using gas chromatography (GC). The CO<sub>2</sub> was detected by thermal conductivity detector (TCD, Shincarbon) and methanol was detected by flame ionization detector (FID, Rtx-5) with conditions in **Table 7**.

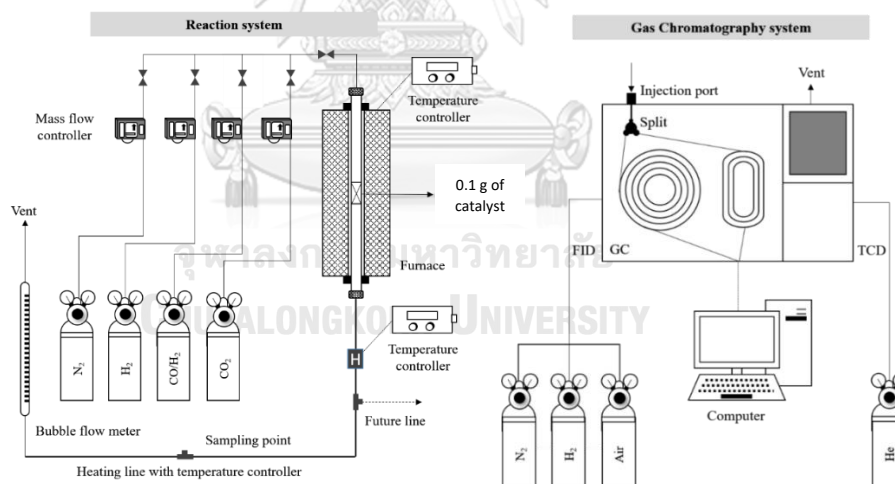


**Figure 8.** Experimental set-up for reaction test



Table 7. The operating condition of gas chromatography

Gas Chromatography	Shimadzu GC-2014 multidetector	
Detector	TCD	FID
Column	Pack-bed column (Shincarbon)	Capillary column (Rtx-5)
Carrier gas	He	N <sub>2</sub> , H <sub>2</sub> , Air
Injector temperature	170 °C	170 °C
Column temperature	(Link FID)	(Link TCD)
- Initial	150 °C	150 °C
- Hold	280 °C	280 °C
- Cool down	150 °C	150 °C
Detector temperature	150 °C	150 °C
Time analysis	15 min	15 min
Analyzed gas	CO, CO <sub>2</sub> , H <sub>2</sub> , N <sub>2</sub>	CH <sub>3</sub> OH, CH <sub>4</sub> , other hydrocarbons

The activity of catalyst is determined by the conversion of CO<sub>2</sub> ( $X_i$ ), selectivity of products ( $S_j$ ) and yield of products ( $Y_j$ ), which can be calculated from the equations as follows:

$$X_i (\%) = \frac{[n_i(in) - n_i(out)] \times 100}{n_i(in)}$$

$$S_j (\%) = \frac{n_j \times 100}{\sum n_j}$$

$$Y_j (\%) = \frac{X_i \times S_j}{100}$$

Where  $n_i(in)$  = the number of mole CO<sub>2</sub> in feed

$n_i(out)$  = the number of mole of non-reacted CO<sub>2</sub>

$n_j$  = the number of mole of each product

#### Part 2: Stability and deactivation

In order to determine the stability and deactivation of each catalyst at the highest selectivity temperature of methanol, the catalyst was tested with hydrogenation of CO<sub>2</sub> as in Part 1, but reacted at the temperature with high methanol selectivity for 5 hours to determine the stability of catalysts over an extended period.

## CHAPTER 4

### RESULTS AND DISCUSSION

In this chapter, characterization, and results of catalyst test in CO<sub>2</sub> hydrogenation are analyzed. It is divided into 3 parts: characterization, temperature-programmed reaction, and time-on-stream reaction.

#### 4.1. Catalysts characterization

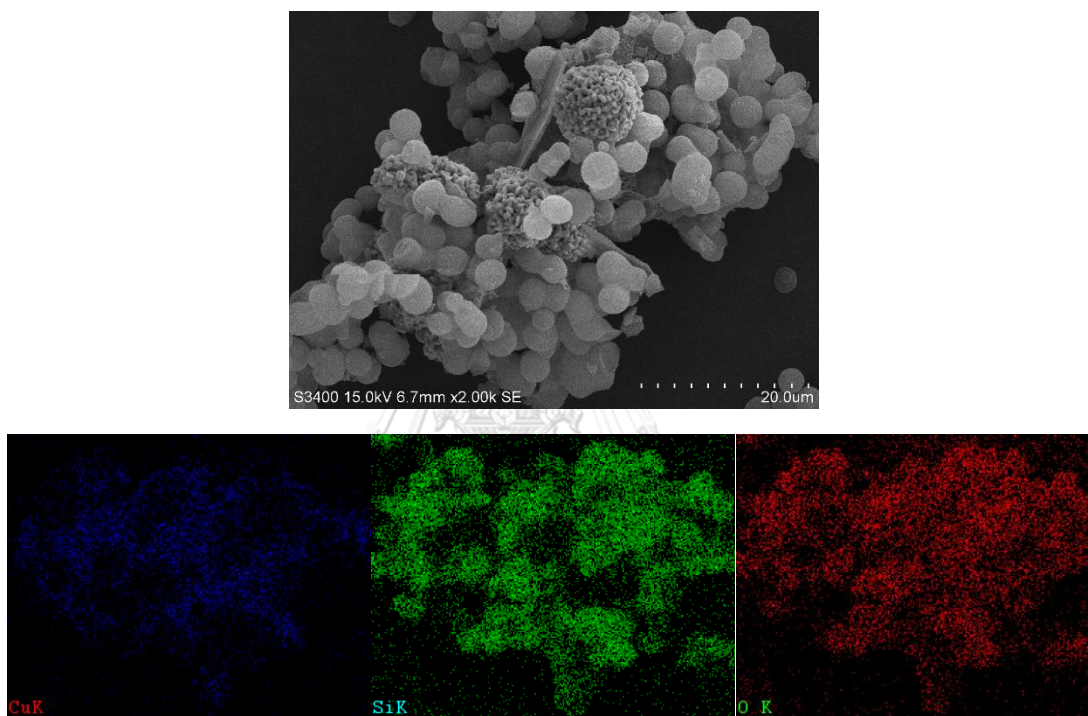


Figure 9. The SEM-EDX images of Cu/MCF-Si (W) catalyst

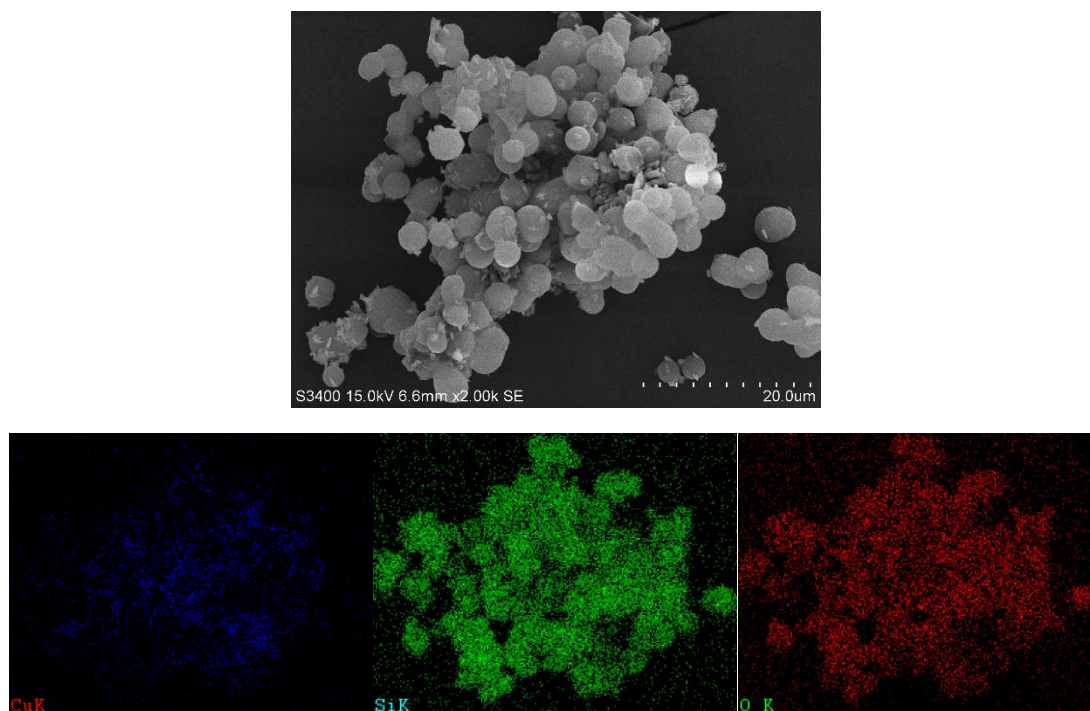


Figure 10. The SEM-EDX images of Cu/MCF-Si (IW) catalyst

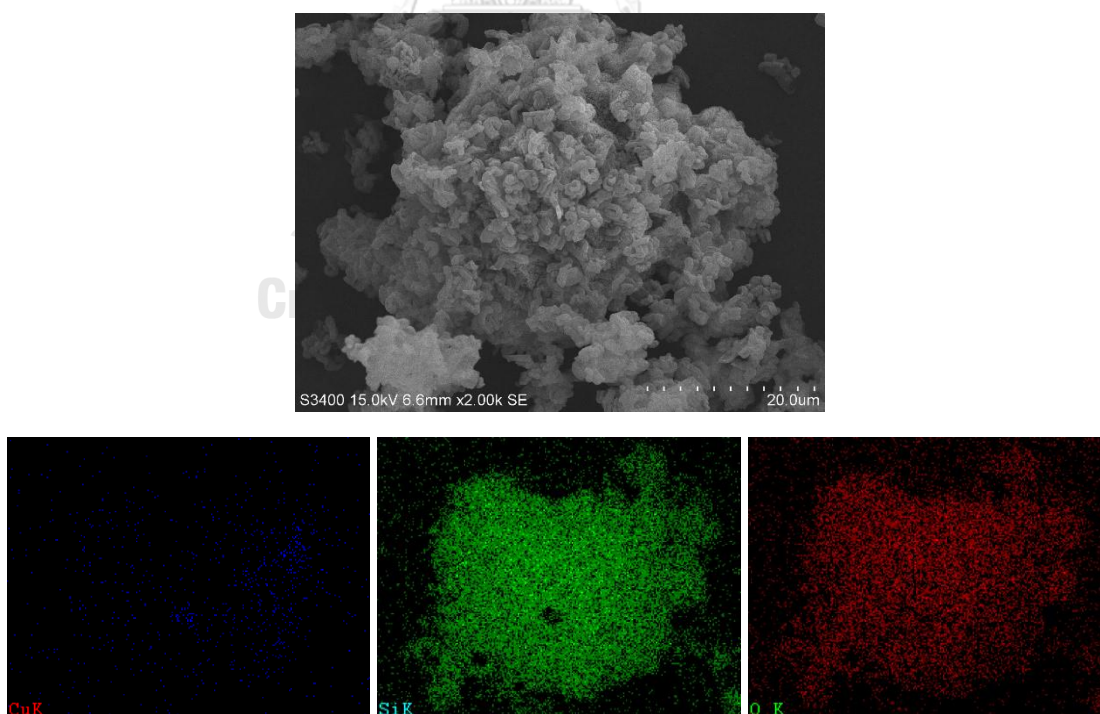
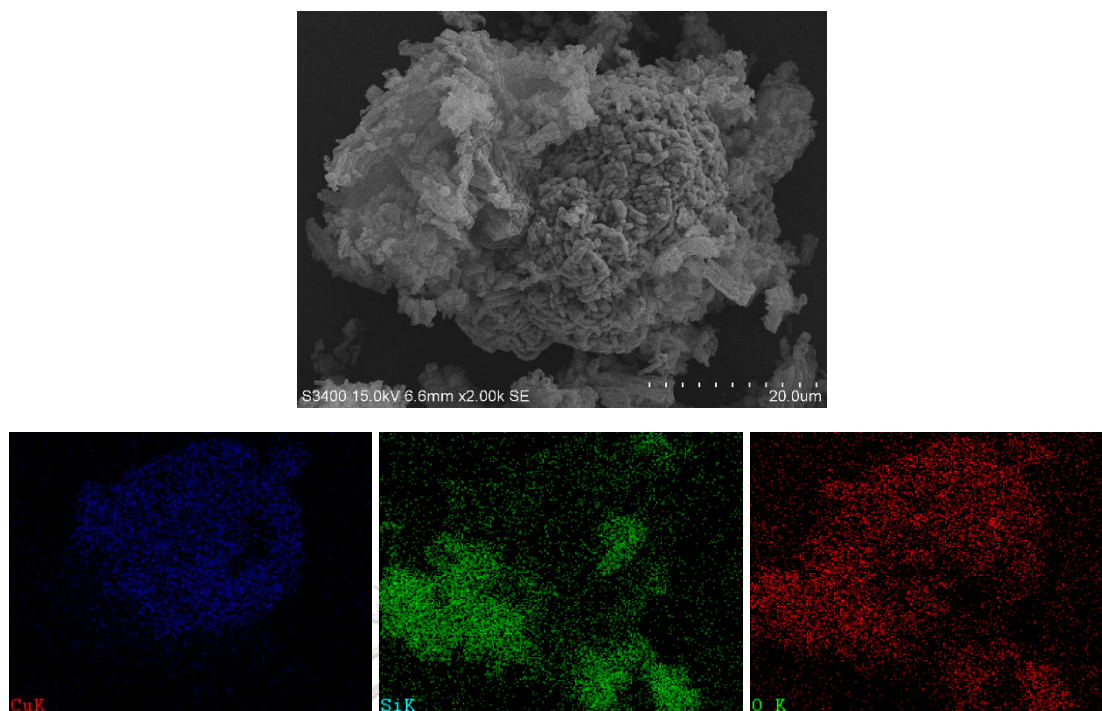


Figure 11. The SEM-EDX images of Cu/SBA-15 (W) catalyst



**Figure 12.** The SEM-EDX images of Cu/SBA-15 (IW) catalyst

The SEM technique was used to analyze the catalyst morphology as shown in **Figure 9-12**. From the SEM micrograph at a magnification of 2.00 k, Cu impregnation on the support did not destroy the morphology of the MCF-Si, but there are some scattered non-impregnated CuO. On the other hand, the morphology of the SBA-15 was not clearly visible because of CuO covering on the support. The EDX technique was used to analyze the elemental distribution on the surface of catalysts (less than 5 microns from surface) as shown in **Figure. 9-12**. From the EDX micrograph, Cu metal was found to be well dispersed on the MCF-Si support surface by two impregnation methods, but in the SBA-15 support, the wetness impregnation method showed much less Cu dispersion, compared with the incipient wetness impregnation method. Corresponding, Cu content on the catalyst surface is shown in Table 8. As analyzed from EDX measurements, it was found that the amount of copper by wt% on the surface of the SBA-15 supports synthesized with the wetness impregnation method was the lowest.

**Table 8.** The elemental distribution of catalysts

Type of catalysts	Cu content (wt%)	
	EDX	XRF
Cu/MCF-Si (W)	40.37	51.93
Cu/MCF-Si (IW)	37.44	51.98
Cu/SBA-15 (W)	16.52	49.47
Cu/SBA-15 (IW)	46.92	59.17

Since elemental distribution studies from EDX analysis are limited, only the amount of Cu near external surface can be studied. Thus, all catalysts were analyzed by XRF method, which is the analysis of all substances in the catalyst bulk. It is shown in **Table 8**. The amount of Cu found is greater than that of the EDX analysis, indicating that in the catalyst impregnation, the Cu precursor penetrates well into the pore, not spread only on the external surface.

The amount of Cu found on the catalyst was less than the amount needed to be impregnated at 60 wt% due to the impregnation method in the moisture removal step. The Cu on the solution floats up to the surface of the solution. When the Cu solution dries, it sticks to the rim of the catalyst container.

However, from theoretical considerations, the Cu content on the substrate with the wetness impregnation method should be greater than the incipient wetness impregnation method because the wetness impregnation method uses water as the solvent and is stirred for adhesion between the Cu precursor and the substrate. Rather than the incipient wetness impregnation method, which is just a drop of Cu precursor coated on the substrate. The result of this experiment is not in accordance with the theory.

The crystal structure of the catalyst was studied with XRD measurement. From **Figure 13**. The low angle XRD pattern analyzed at  $2\theta = 0.5^\circ\text{-}5^\circ$  revealed that the synthesized substances actually form mesoporous silica materials, types of MCF-Si and SBA-15. In addition, MCF-Si has a major peak at  $2\theta = 0.4^\circ$ , which represents a spherical structure[40], while SBA-15 has three peaks at the (100), (110) and (200) indexes, where these peaks represent highly ordered two-dimensional hexagonal mesoporous structure [41]. It can also be confirmed that the catalyst structure still resembles a pre-Cu-impregnated support. In other words, both methods of Cu impregnation did not destroy the structure of the mesoporous silica supports.

The wide-angle XRD is used to analyze the crystal size. Analyzing at  $2\theta = 10^\circ\text{-}80^\circ$  from XRD patterns in **Figure 14**. shown that  $\text{Cu}^{2+}$  is formed, by observing the peak characterizing CuO at the position  $2\theta = 32.67^\circ, 35.63^\circ, 38.90^\circ, 48.83^\circ, 53.60^\circ, 58.24^\circ, 61.59^\circ, 66.5^\circ$  and  $68.19^\circ$  on the catalyst[42] and no peaks of  $\text{Cu}_2\text{O}$  appear at  $2\theta = 43.28^\circ, 50.40^\circ$  and  $74.81^\circ$ [43]. Compared with XRD patterns of MCF-Si and SBA-15 supports, it showed  $\text{SiO}_2$  peaks at  $2\theta = 21.8^\circ$  [44] indicating that amorphous was decreased. It was shown that the Cu impregnation decreased the amorphous of the supports, which no significant differences due to different impregnation methods. Additionally, the crystallite size of CuO can be calculated from the Scherrer's equation as shown in **Table 9**. This showed that the crystallite size of catalysts was similar.

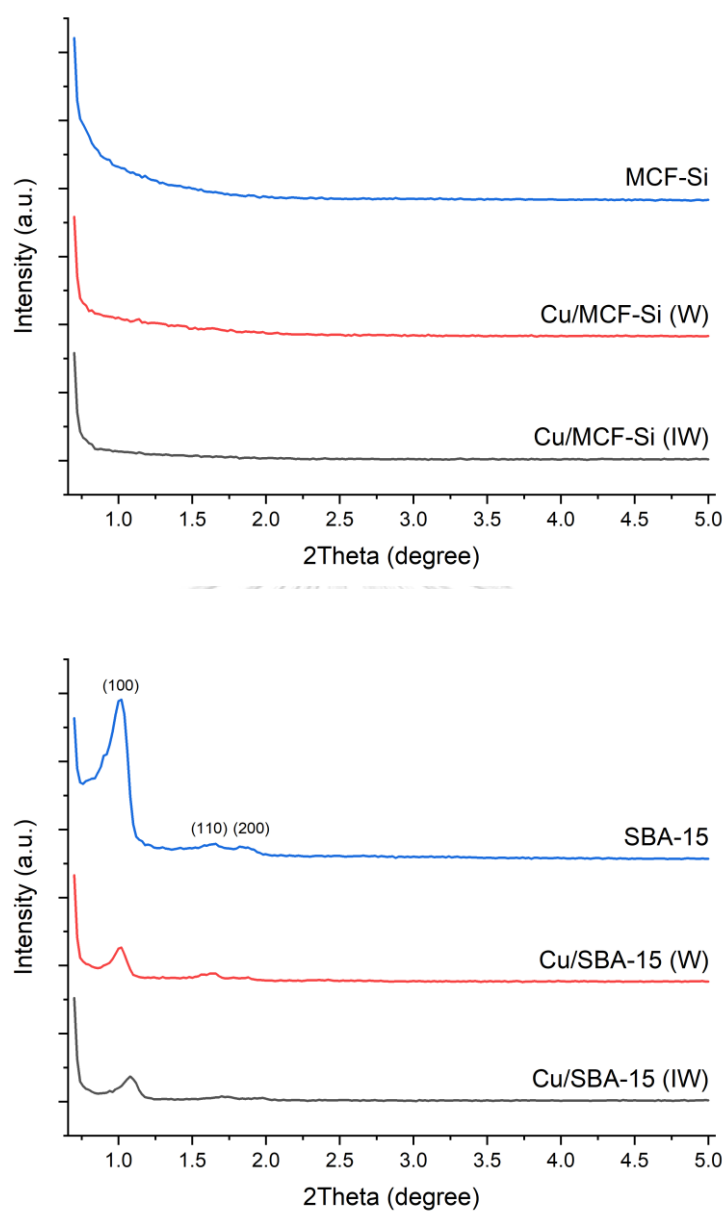
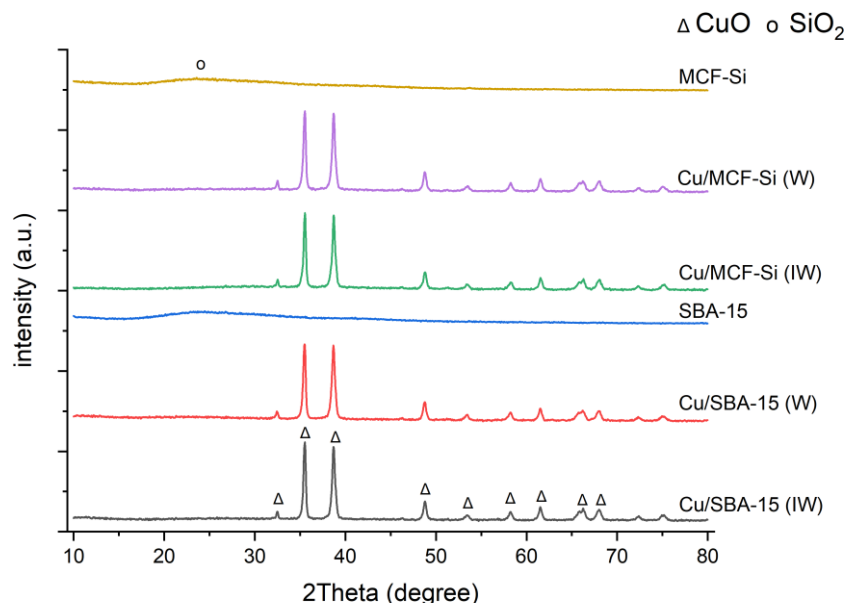


Figure 13. The low-angle XRD patterns of the MCF-Si supported (above) and the SBA-15 supported (below) catalysts





**Figure 14.** The wide-angle XRD patterns of the catalysts

**Table 9.** The crystallite size calculated from Scherrer's equation

Type of catalysts	Crystallite size of CuO, $D_{Cu}$ (nm)
Cu/MCF-Si (W)	21
Cu/MCF-Si (IW)	20
Cu/SBA-15 (W)	22
Cu/SBA-15 (IW)	21

The TEM analysis was applied to study the pore structure on the catalyst. **Figure 15-16** show the TEM micrograph at a magnification of 100k indicating that the pore structure on the MCF-Si catalyst was 3-dimensional spherical structures [45], whereas SBA-15 TEM images show two-dimensional hexagonal structures [46]. No significant differences were observed due to different impregnation methods. Meanwhile, the TEM analysis images show the crystallite size, which is consistent with the results from XRD analysis using the Scherrer's equation as seen in **Table 9**, in which the crystallite size was approximately 20 nm.

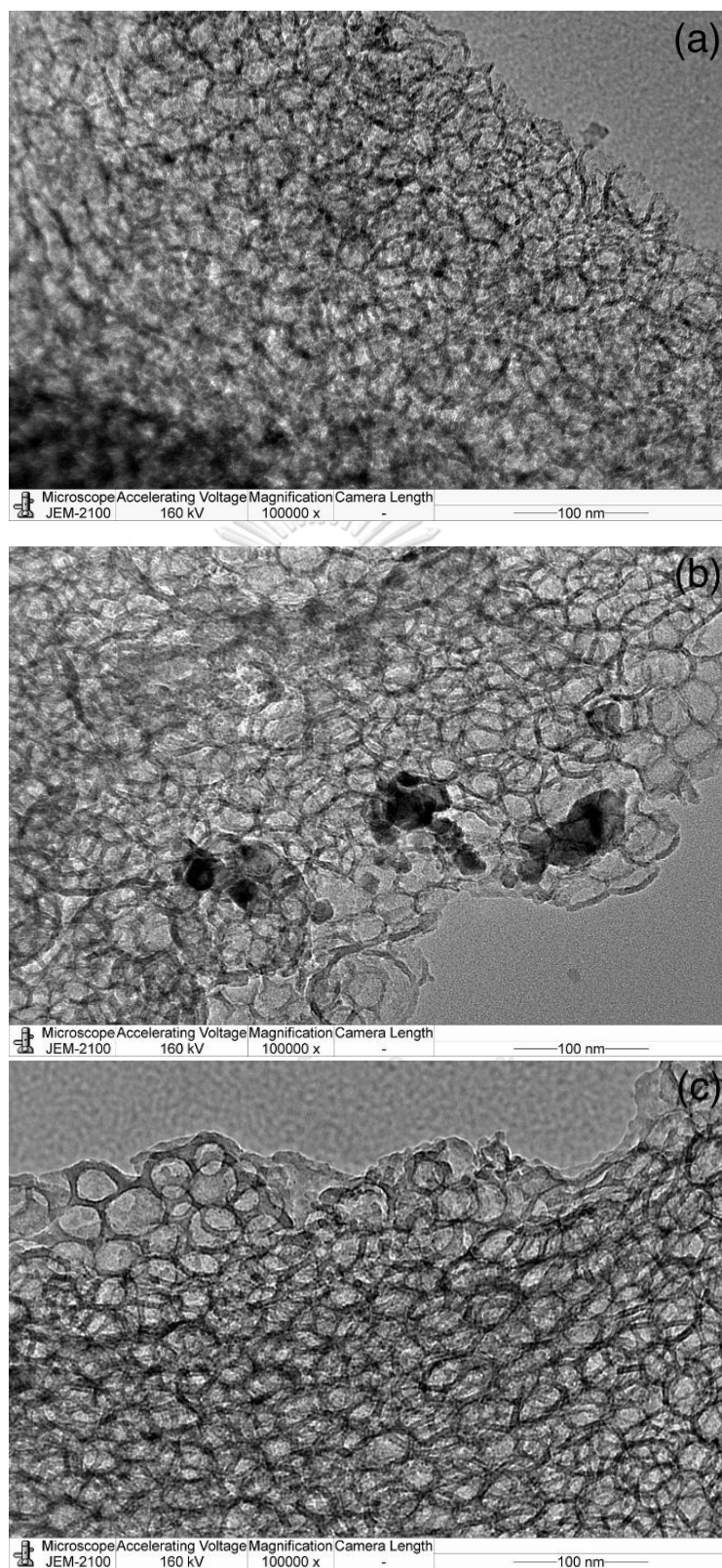


**Figure 15.** The TEM micrograph of (a) MCF-Si, (b) Cu/MCF-Si (W) and (c) Cu/MCF-Si (IW) catalysts

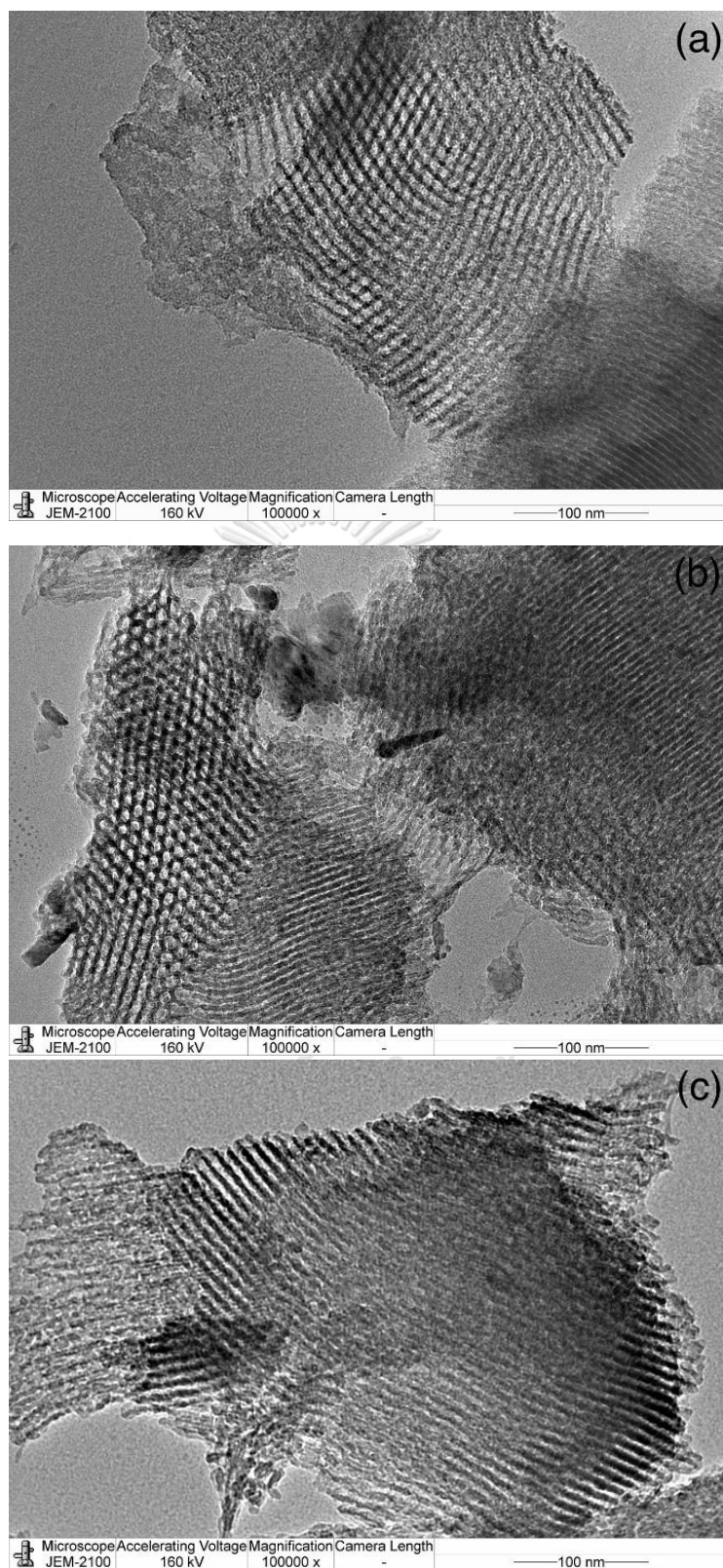


**Figure 16.** The TEM micrograph of (a) SBA-15, (b) Cu/SBA-15 (W) and (c) Cu/SBA-15 (IW) catalysts

**Table 10.** The BET surface area, pore volume and average pore diameter of catalysts

Type of catalysts	BET surface area <sup>a</sup> (m <sup>2</sup> /g)	Pore volume <sup>b</sup> (cm <sup>3</sup> /g)	Average pore diameter <sup>b</sup> (nm)
MCF-Si	464	0.7	6.0
Cu/MCF-Si(W)	159	0.4	11.0
Cu/MCF-Si(IW)	158	0.4	9.8
SBA-15	461	1.2	10.6
Cu/SBA-15(W)	175	0.3	7.9
Cu/SBA-15(IW)	175	0.3	6.1

<sup>a</sup> Determined from BET method

<sup>b</sup> Determined from BJH desorption method

The N<sub>2</sub> physisorption was used to determine the surface area, pore volume and average pore diameter as shown the results in **Table 10**. The analysis results from the BET method showed that when the Cu was impregnated, the surface area was decreased. Both impregnation methods including wetness impregnation and incipient wetness impregnation method had the same surface area. This revealed that the impregnation methods did not affect the amount of surface area. Meanwhile, the analysis results from the BJH method showed that after Cu was impregnated, the pore volume was decreased by both impregnation methods, corresponding to the surface area. However, from the pore size distribution analysis, it was found that after Cu impregnation, the pore size of MCF-Si was smaller and the pore size of the SBA-15 was larger. By wetness impregnation method, the pore size distribution was larger than incipient wetness impregnation method.

N<sub>2</sub> physisorption profiles are displayed in **Figure 17**, demonstrating type IV isotherms [47] as defined by the IUPAC. Type IV isotherms are decreased by Cu impregnation. The catalyst with an MCF-Si support showed more type IV isotherms than an SBA-15 support. The results of the impregnation method showed that the wetness impregnation method (W) had better type IV isotherms than the incipient wetness impregnation method, corresponding to the pore size distribution.

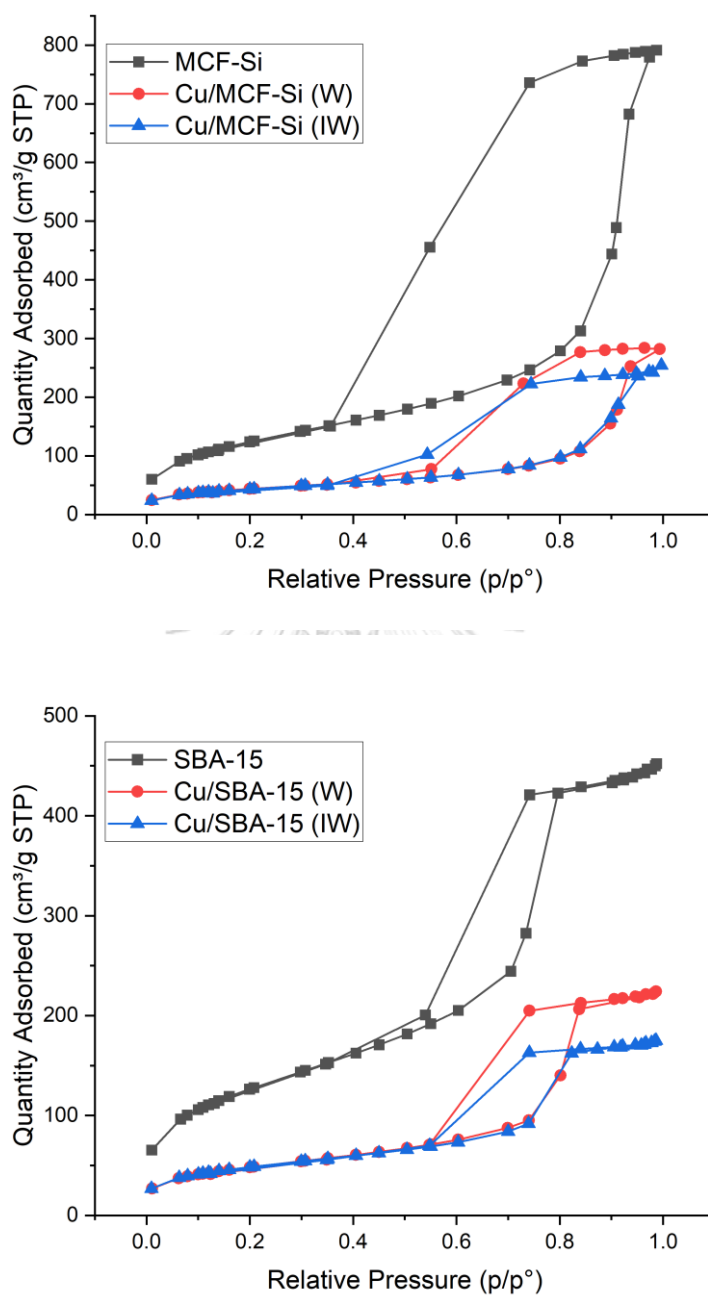


**Figure 17.** N<sub>2</sub> physisorption isotherms of MCF-Si and MCF-Si supported catalysts (above) and SBA-15 and SBA-15 supported catalysts (below)

The number of surface active sites and active site dispersion were analyzed by CO-chemisorption method as shown in **Table 11**. The SBA-15 supported catalysts had more surface active sites than the MCF-Si supported catalysts, which was consistent with the BET analysis, and the incipient wetness impregnation had more surface active sites than the wetness impregnation. This was consistent with active site distribution where the incipient wetness impregnation method was more dispersible than the wetness impregnation method. At the same time, the type of support did not significantly affect the distribution of active sites.

Table 11. The surface active site ( $S_{Cu}$ ) and the active sites dispersion (D)

Type of catalysts	$S_{Cu}$ (m <sup>2</sup> /g)	D (%)
Cu/MCF-Si (W)	8.6	9.11
Cu/MCF-Si (IW)	11.4	12.01
Cu/SBA-15 (W)	9.8	10.37
Cu/SBA-15 (IW)	11.0	11.58

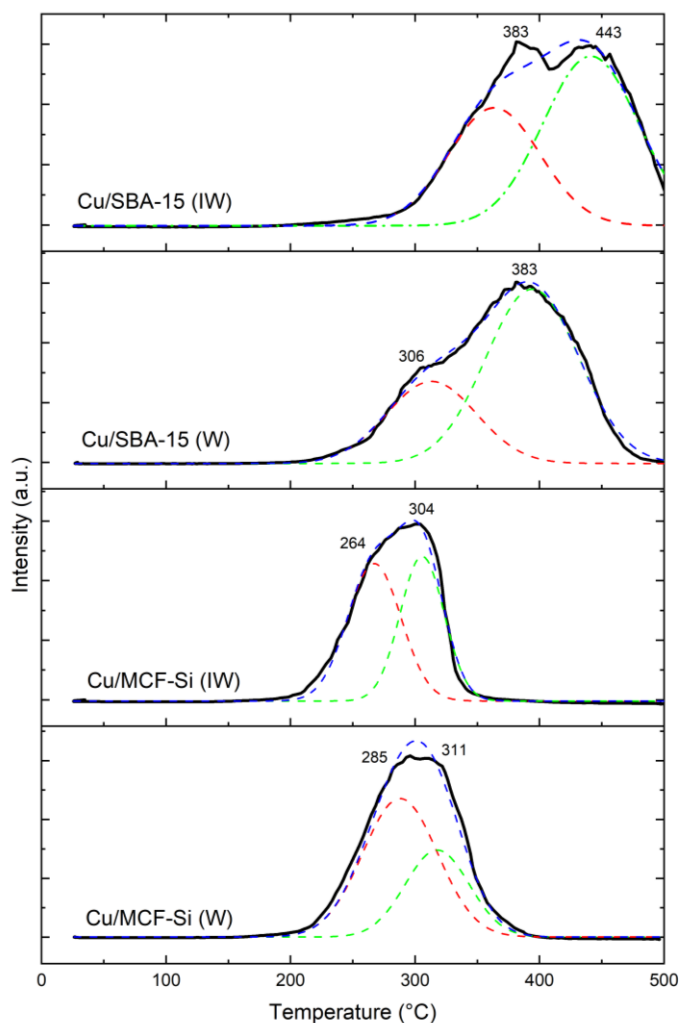


**Figure 18.** Temperature programmed reduction ( $H_2$ -TPR) of catalysts

The reduction behavior of the catalyst is shown in **Figure 18**. In this analysis, only CuO is analyzed, since  $SiO_2$  can be reduced at temperatures above 1500 °C [48]. The MCF-Si supported catalysts are reduced at approximately 300°C, but the SBA-15 supported catalysts are reduced at approximately 380°C. The reason that the MCF-Si supported catalysts are more efficient at reducing is due to their morphology. In the MCF-Si supported catalyst, CuO molecules were found, but in the SBA-15 supported catalyst, the CuO molecules were enclosed in clusters. So, the reducibility of Cu-based catalysts impregnated on MCF-Si was more than SBA-15.

## 4.2. Screening catalysts

To study the efficiency of the catalyst, the CO<sub>2</sub> hydrogenation reaction was conducted at 100-400 °C, pressure 10 bar, CO<sub>2</sub>: H<sub>2</sub> ratio = 1:3, CO<sub>2</sub> conversion and methanol selectivity were obtained at various temperatures to study the optimum temperature for the reaction. The result is shown in **Figure 19**. The figure shows the disappearance of CO<sub>2</sub> converted to CO by the reverse water-gas shift (RWGS) reaction. Then, CO reacts with H<sub>2</sub>O to form methanol in the CO hydrogenation reaction as shown the selectivity in **Table 12**.

**Figure 19**. shows that CO<sub>2</sub> conversion tends to increase with increasing temperature. In the other hand, when the temperature rises, the reaction to convert CO<sub>2</sub> to CO by RWGS reaction was better. The catalyst with the highest CO<sub>2</sub> conversion was Cu/MCF-Si (W), followed by Cu/MCF-Si (IW), Cu/SBA-15 (W), and Cu/SBA-15 (IW), respectively. The reason for the MCF-Si supported catalyst has a higher CO<sub>2</sub> conversion is because the catalyst uses a lower reduction temperature. Therefore, the catalyst is more converted from CuO to Cu<sup>0</sup>. The RWGS reaction is more possible when an efficient catalyst is involved. Meanwhile, catalysts supported with SBA-15 undergo reduction at temperatures above 300°C, so the catalyst is inefficient or less active site as Cu<sup>0</sup> enough to increase conversion of CO<sub>2</sub> to CO. The results of the CO<sub>2</sub> conversion were consistent with the results of the catalyst reduction temperature that obtained by H<sub>2</sub>-TPR analysis as shown in **Figure 18**.

CO and methanol selectivity shown in **Table 12**. also indicated the effect of CO hydrogenation reaction after RWGS reaction and CO<sub>2</sub> hydrogenation. The methanol was formed in the catalyst supported by MCF-Si at 300 and 400 °C, but in the catalyst supported on SBA-15, methanol was formed only at 400 °C because of high temperature reduction, at 300 °C, the initial reduction temperature of the SBA-15 supported catalyst. So, CO cannot react with H<sub>2</sub> to form methanol at 300 °C.

As for the catalyst supported with MCF-Si, when the temperature was increased, methanol selectivity was decreased. This conflicts with CO<sub>2</sub> conversion because of the RWGS reaction, which converts CO<sub>2</sub> to CO, is endothermic. In other words, as the temperature increases, the reaction proceeds forward [49]. However, the CO hydrogenation reaction to methanol is an exothermic reaction, that is, when the



temperature increases, the reaction progresses even worse. For this reason, when the temperature increases therefore, methanol selectivity decreased.

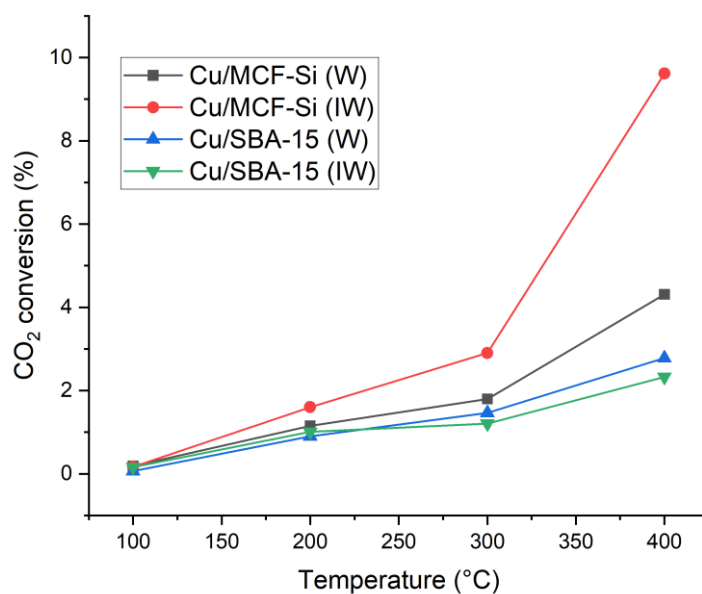


**Figure 19.** The CO<sub>2</sub> conversion of catalysts reacted at 100-400 °C

**Table 12.** The CO and methanol selectivity of catalysts at 300 and 400 °C

Catalysts	CO selectivity		MeOH selectivity	
	Temperature (C°)		Temperature (C°)	
	300	400	300	400
Cu/MCF-Si (W)	99.16	99.71	0.84	0.29
Cu/MCF-Si (IW)	99.24	99.85	0.76	0.15
Cu/SBA-15 (W)	100	99.76	0	0.24
Cu/SBA-15 (W)	100	99.67	0	0.33

### 4.3. Catalysts stability

The stability of the catalyst can be studied through time-on-stream CO<sub>2</sub> Hydrogenation or reaction at the same temperature, pressure, and ratio for a specified period of time. To study the CO<sub>2</sub> condition and methanol selectivity at different times while the reaction was going on.

**Figure 20.** presents the CO<sub>2</sub> conversion of catalysts during time-on-stream for CO<sub>2</sub> hydrogenation at 400 °C, pressure 10 bar, CO<sub>2</sub>:H<sub>2</sub> ratio = 1:3 for 5 hours. From graph, the CO<sub>2</sub> conversion of catalyst Cu/MCF-Si (IW) was the highest, followed by Cu/MCF-Si (W), Cu/SBA-15 (IW) and Cu/SBA-15 (W), respectively, which was consistent with the results from the screening of catalyst part. The MCF-Si supported catalyst had a higher CO<sub>2</sub> conversion than the SBA-15 supported catalyst based on the reduction behavior. Over the time of 5 hours, CO<sub>2</sub> conversions did not tend to decrease, demonstrating that the stability of all types of catalysts was good.

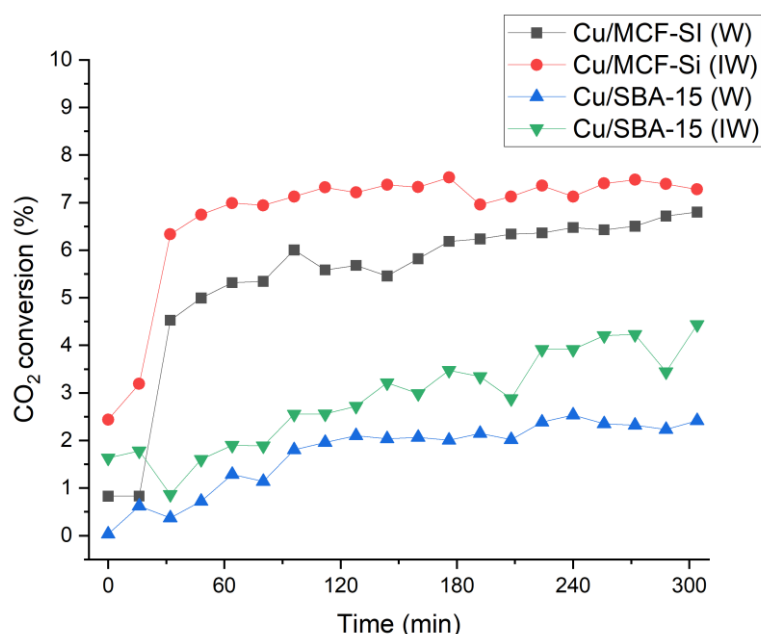


**Figure 20.** The CO<sub>2</sub> conversion during time-on-stream of CO<sub>2</sub> hydrogenation for 5 hours at 400 °C.

#### 4.4. Catalysts deactivation

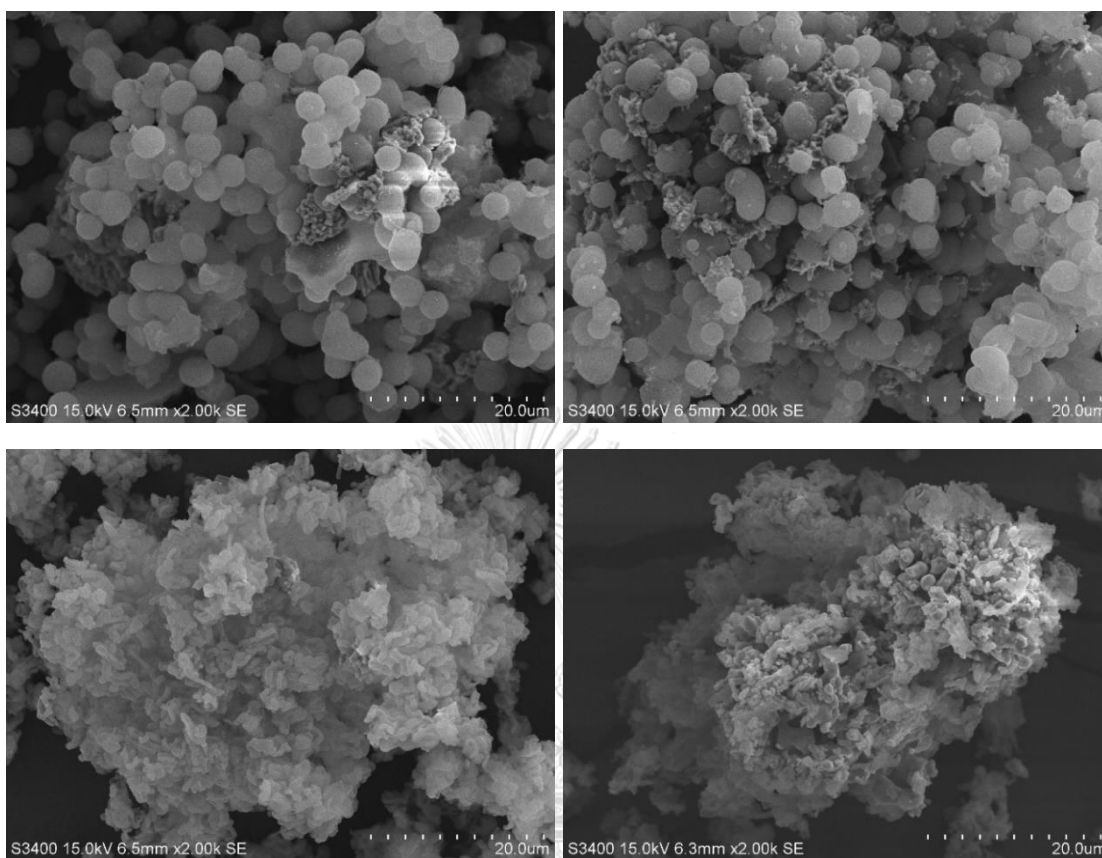


**Figure 21.** The SEM micrograph of (a) Cu/MCF-Si (W), (b) Cu/MCF-Si (IW), (c), Cu/SBA-15 (W) and (d) Cu/SBA-15 (IW)

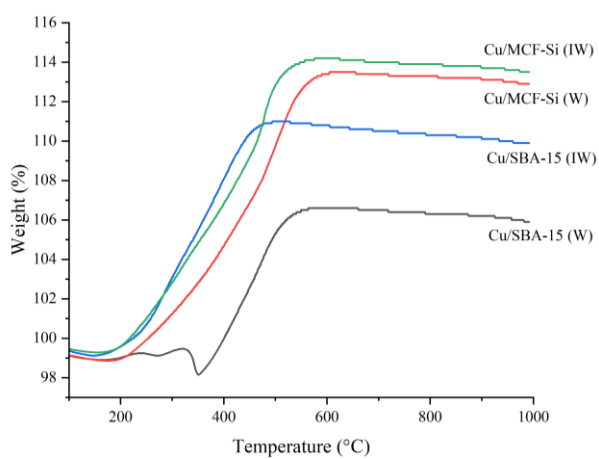


**Figure 22.** The temperature programmed profile of spent catalysts after CO<sub>2</sub> hydrogenation for 5 hours at 400 °C.

From **Figure 23**, SEM images show the catalyst morphology after 5 hours of CO<sub>2</sub> hydrogenation. The spent MCF-Si supported catalyst was the same as fresh one. In other words, the structure of the support was not destroyed. But in the SBA-15 supported catalyst, the CuO covering around the support was more dispersed. This makes the structure of the support clearly visible, and the Cu impregnation method has no significant effect.

The catalyst deactivation analysis can be studied by TG analysis. From **Figure 24**, it was found that the %weight of all catalysts increased. The increase of %weight is caused by the fact that in spent catalysts, there are Cu<sup>0</sup> atoms left over from the reduction pretreatment before the reaction. This Cu<sup>0</sup> oxidizes with O<sub>2</sub> in air to form CuO molecules, increasing the weight of the catalyst [50]. From the analysis of H<sub>2</sub>-TPR as shown in **Figure 18**, Cu/SBA-15 (W) catalyst was used for high temperature reduction at 383 °C. Therefore, in pretreating the catalyst at 300 °C before reaction, the reduction reaction to convert CuO to Cu<sup>0</sup> was not all possible. Therefore, Cu<sup>0</sup> was not found in the catalyst and in the absence of Cu<sup>0</sup> a %weight was decreased until the temperature around 380 °C. When the temperature rises to about 380 °C, Cu/SBA-15 (W) undergoes reduction reaction with H<sub>2</sub> in air, producing Cu<sup>0</sup>. Then Cu<sup>0</sup> then oxidation with O<sub>2</sub> in air, forming CuO molecules, causing the %weight of the reaction to begin to increase and increasing steadily at temperatures above 380 °C.

## CHAPTER 5

### CONCLUSIONS AND RECOMENDATIONS

All of catalysts were synthesized including Cu/MCF-Si (W), Cu/MCF-Si (IW), Cu/SBA-15 (W) and Cu/SBA-15 (IW). Cu precursor can be dispersed both on the surface and inside the pore. Except for Cu/SBA-15 (W) catalysts, where Cu distribution was low on the surface, CuO was found in all catalysts with very similar crystallite sizes. Both impregnation methods did not change the porous structure of the supports. The SBA-15 supported catalyst had a greater surface area than MCF-Si, while MCF-Si had better pore volume, pore size distribution and isotherm IV type than SBA-15. The incipient wetness impregnation method has higher surface active site and active site dispersion values than the catalyst synthesized by wetness impregnation method. Cu/MCF-Si (W) has a lower reduction temperature of the catalysts, followed by Cu/MCF-Si (IW), Cu/SBA-15 (W) and Cu/SBA-15 (IW), respectively.

The CO<sub>2</sub> hydrogenation reaction by all four catalysts began at 200 °C. The RWGS reaction between CO<sub>2</sub> and H<sub>2</sub> on Cu<sup>0</sup>, which appeared after reduction, before CO hydrogenation continued at 300 °C for MCF-Si supported catalysts and 400 °C for SBA-15 supported catalysts until methanol was obtained. The decreases of CO<sub>2</sub> in the system indicated that the RWGS reaction had proceeded. It depended on the reduction behavior of the catalyst. Different impregnation methods did not significantly affect the reduction behavior. However, the catalyst supported with MCF-Si uses a lower reducing temperature than that of SBA-15. The results of CO<sub>2</sub> conversion were consistent with the reduction behavior analysis, but when increasing temperature, methanol selectivity decreased because the CO hydrogenation reaction is exothermic. Therefore, methanol selectivity was reversed with the results from the reduction behavior analysis and RWGS reaction. Finally, when comparing the methanol selectivity and CO selectivity, it was found that all catalysts were suitable for the RWGS reaction more than CO<sub>2</sub> hydrogenation to methanol.

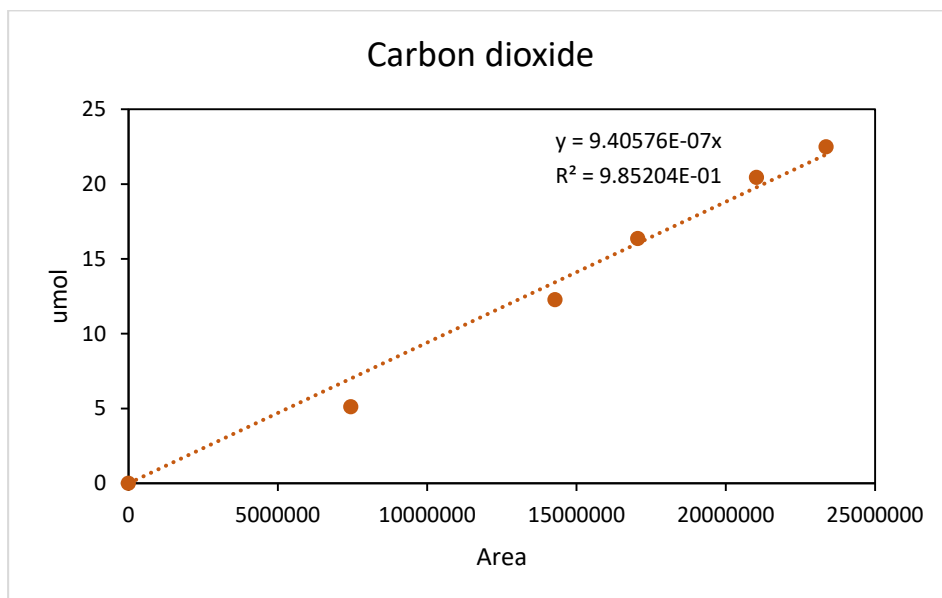
The CO<sub>2</sub> conversion of the catalyst followed the same reduction behavior as mentioned in part 2. It was constant throughout the reaction for 5 hours. Thus, all catalysts were stable to the RWGS reaction. Meanwhile, the MCF-Si supported catalysts yielded stable methanol selectivity over 5 hours, unlike the SBA-15 supported catalysts, the methanol selectivity was initially higher, but as the reaction progressed, the methanol selectivity continued to decrease. This indicated that the catalysts supported with SBA-15 is unstable to CO hydrogenation. However, all these synthesized catalysts were not inferior in performance to CZA commercial catalysts.

### RECOMENDATIONS

1. The wetness impregnation method used in this study is incorrect. The correct method is after stirring, the substance must be filtered out of the solvent prior to dehydrating to remove the solvent. The filtered solvent must be measured for the Cu content to subtract from the initial Cu precursor and calculate the amount of copper on the support.
2. It is interesting to study the optimum amount of Cu for impregnation in each type of support.
3. The addition of promoters such as Zn and Al may able to increase the methanol selectivity.
4. Changing the catalyst reducing temperature experiment affects the efficiency of each catalyst.
5. Studies on the deactivation of spent catalysts should be investigated further with other methods such as XRF because of effects of Cu oxidation.

## APPENDIX

## APPENDIX A. CALIBRATION

A.1. CO<sub>2</sub> calibrationFig. A.1.1. the calibration of CO<sub>2</sub>

## A.2. CO calibration

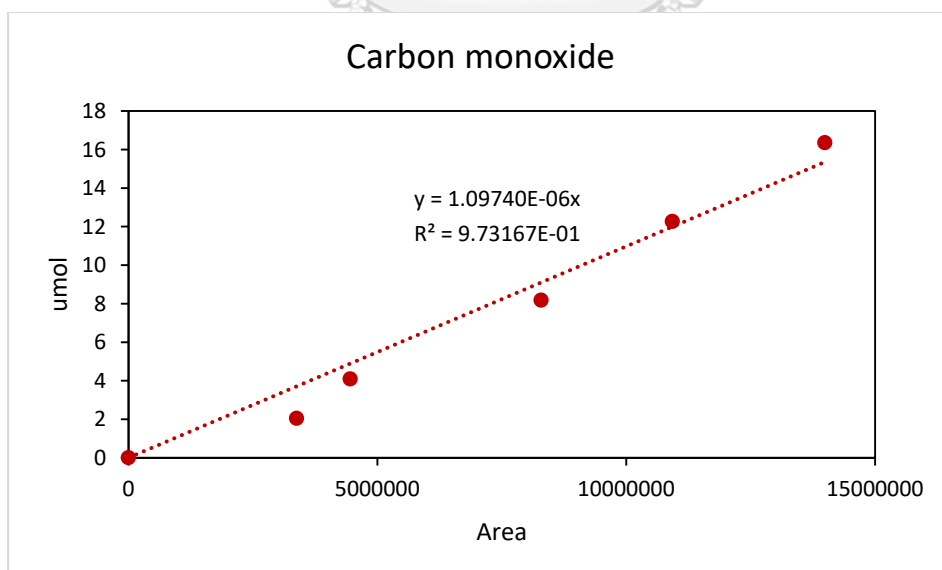


Figure A.2.1. the calibration of CO

## A.3. Methanol calibration

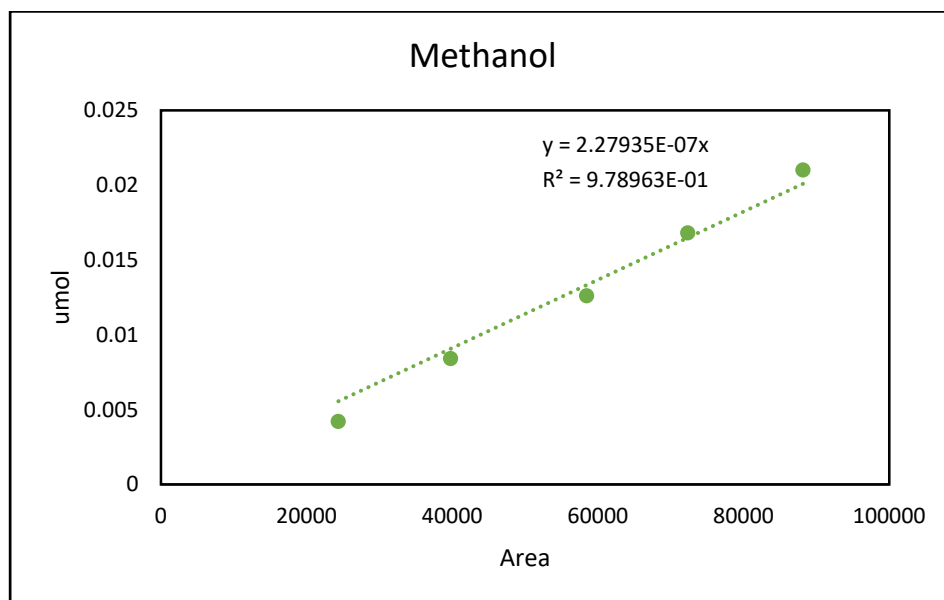


Figure A.3.1. The methanol calibration





## APPENDIX B. CALCULATION OF CATALYST PROPERTIES

B.1. CO<sub>2</sub> conversion

$$\text{CO}_2 \text{ conversion (\%)} = \frac{\text{CO}_{2,\text{in}} - \text{CO}_{2,\text{out}}}{\text{CO}_{2,\text{in}}} \times 100$$

## B.2. Methanol selectivity

$$\text{MeOH selectivity (\%)} = \frac{\text{mole of methanol}}{\text{all products}} \times 100$$

## B.3. CO selectivity

$$\text{CO selectivity (\%)} = \frac{\text{mole of CO}}{\text{all products}} \times 100$$

## B.4. Methanol yield

$$\text{CH}_3\text{OH yield (\%)} = \frac{\text{CH}_3\text{OH selectivity (\%)} \times \text{conversion (\%)}}{100}$$

Table B.4.1 methanol yield of CO<sub>2</sub> hydrogenation in various temperature

Catalysts	Methanol yield (%)			
	100°C	200°C	300°C	400°C
CZA	0	0.637	0.052	0.013
Cu/MCF-Si (W)	0	0	0.015	0.012
Cu/MCF-Si (IW)	0	0	0.022	0.014
Cu/SBA-15 (W)	0	0	0	0.007
Cu/SBA-15 (W)	0	0	0	0.008

Table B.4.2 methanol yield of CO<sub>2</sub> hydrogenation at 400 °C for 5 hours

Time (min)	Methanol yield (%)				
	CZA	Cu/MCF-Si (W)	Cu/MCF-Si (IW)	Cu/SBA-15 (W)	Cu/SBA-15 (IW)
0	0.002	0.001	0.001	0.000	0.003
16	0.001	0.001	0.003	0.000	0.006
32	0.021	0.009	0.006	0.001	0.003
48	0.036	0.011	0.006	0.001	0.005
64	0.028	0.011	0.007	0.004	0.006
80	0.027	0.011	0.006	0.003	0.005
96	0.027	0.012	0.007	0.005	0.007
112	0.028	0.010	0.007	0.006	0.007
128	0.032	0.011	0.007	0.006	0.007
144	0.030	0.011	0.007	0.006	0.007
160	0.026	0.011	0.006	0.005	0.007
176	0.026	0.012	0.007	0.005	0.008
192	0.027	0.012	0.006	0.006	0.007
208	0.033	0.012	0.006	0.005	0.006
224	0.032	0.012	0.006	0.006	0.008
240	0.057	0.012	0.006	0.006	0.008
256	0.040	0.012	0.007	0.006	0.008
272	0.053	0.012	0.007	0.005	0.008
288	0.037	0.013	0.007	0.005	0.006
304	0.037	0.012	0.007	0.005	0.008

## APPENDIX C. CALCULATION OF CRYSTALLITE SIZE

The Scherrer equation

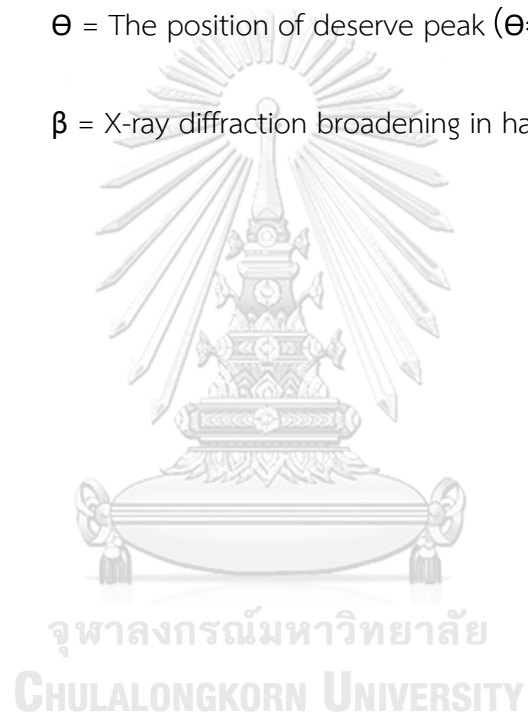
$$D = \frac{k\lambda}{\beta \cos\theta}$$

Where; D = Volume average crystallite size

K = unity constant factor (k=0.9)

$\theta$  = The position of deserve peak ( $\theta=1.5406$ )

$\beta$  = X-ray diffraction broadening in half peak (radian)



## APPENDIX D. CO-CHEMISORPTION

D.1. Calculation the surface active sites

$$MSA_s = S_f \times \frac{V_{ads}}{V_g} \times \frac{100\%}{\%M} \times N_A \times \sigma_m \times \frac{m^2}{10^{18}nm^2}$$

Where  $MSA_s$  = surface-active sites $S_f$  = stoichiometry factor $V_{ads}$  = volume adsorbed, (cm<sup>3</sup>/g) $V_g$  = molar volume of gas at STP, 22414 (cm<sup>3</sup>/mol) $N_A$  = Avogadro's number, 6.023x10<sup>23</sup> (molecules/mol) $\sigma_m$  = cross-sectional area of active metal atom, (nm<sup>2</sup>)

D.2. Calculation the dispersion of active sites

$$D(\%) = S_f \times \frac{V_{ads}}{V_g} \times \frac{m. w.}{\%M} \times 100\%100\%$$

Where  $D(\%)$  = active site dispersion $S_f$  = stoichiometry factor $V_{ads}$  = volume adsorbed, (cm<sup>3</sup>/g) $V_g$  = molar volume of gas at STP, (22414 cm<sup>3</sup>/mol)

m.w. = molecular weight of the metal, (a.m.u.)

 $\%M$  = %metal, (%)

## D.3. Calculation the volume chemisorbed

$$V_{\text{ads}}(\text{cm}^3) = \frac{V_{\text{inj}}}{m} \times \sum_{i=1}^n \left(1 - \frac{A_i}{A_f}\right)$$

Where  $V_{\text{inj}}$  = volume injection ( $\text{cm}^3$ )

$M$  = mass of sample (g)

$A_i$  = area of peak  $i$

$A_f$  = area of last peak

Table D.3.1. The area of peak of Cu/MCF-Si (W) catalyst adsorbed CO gas

Peak no.	Area			
	Cu/MCF-Si (W)	Cu/MCF-Si (IW)	Cu/SBA-15 (W)	Cu/SBA-15 (IW)
1	0.12609	0.12865	0.13554	0.13122
2	0.13069	0.12105	0.12846	0.12642
3	0.12520	0.12431	0.11159	0.13029
4	0.13546	0.11226	0.12465	0.11593
5	0.12001	0.12011	0.11849	0.11206
6	0.13319	0.14199	0.11405	0.12176
7	0.12429	0.09593	0.14130	0.11030
8	0.12396	0.11677	0.12001	0.11839
9	0.12681	0.13257	0.13096	0.12484
10	0.13923	0.11263	0.13342	0.10998
11	0.13975	0.10022	0.14008	0.12696
12	0.14077	0.14769	0.14360	0.1189
13	-	0.12016	0.14395	0.11501
14	-	0.15103	0.14416	0.13488
15	-	0.15153	-	0.13543
16	-	0.15347	-	0.13576

## REFERENCES

### Reference

1. United States Environmental Protection Agency, *Overview of Greenhouse Gasses*. 2007, IPCC (2007) Climate change 2007: The physical Science Basis.
2. Guil-López, R., et al., *Methanol Synthesis from CO<sub>2</sub>: A Review of the Latest Developments in Heterogeneous Catalysis*. Materials (Basel), 2019. **12**(23).
3. Yang, Y., M.G. White, and P. Liu, *Theoretical Study of Methanol Synthesis from CO<sub>2</sub> Hydrogenation on Metal-Doped Cu(111) Surfaces*. The Journal of Physical Chemistry C, 2012. **116**(1): p. 248-256.
4. Liang, B., et al., *Investigation on Deactivation of Cu/ZnO/Al<sub>2</sub>O<sub>3</sub> Catalyst for CO<sub>2</sub> Hydrogenation to Methanol*. Industrial & Engineering Chemistry Research, 2019. **58**(21): p. 9030-9037.
5. Maria, V., B. Francisco, and A. Daniel, *Mesoporous material for Drug Delivery*. Angewandte chemie, 2007. **46**: p. 7548-7558.
6. Information, N.C.f.B. *Carbon dioxide*. 2022 [cited 2022; Available from: <https://pubchem.ncbi.nlm.nih.gov/compound/Carbon-dioxide>].
7. information, N.c.f.B. *Methanol*. Available from: <https://pubchem.ncbi.nlm.nih.gov/compound/Carbon-dioxide#section=Vapor-Phase-IR-Spectra>.
8. KGaA., M. *Mesoporous material synthesis* Available from: <https://www.sigmaaldrich.com/TH/en/technical-documents/technical-article/materials-science-and-engineering/tissue-engineering/mesoporous-materials>.
9. Hermida, L., et al., *Review of large-pore mesostructured cellular foam (MCF) silica and its applications*. Open Chemistry, 2019. **17**: p. 1000-1016.
10. Material, A. *SBA-15*. Available from: <https://www.acsmaterial.com/sba-15-20g.html>.
11. Ching, C.Y., *Synthesis and Characterization of Santa Barbara Amorphous*

(SBA-15) for CO<sub>2</sub>/CH<sub>4</sub> Separation. 2015, UNIVERSITI TEKNOLOGI PETRONAS.

12. Pompe, C., et al., *Stability of Mesocellular Foam Supported Copper Catalysts for Methanol Synthesis*. *Catalysis Today*, 2019. **334**.
13. Yu, Y.M., et al., *MCM-41 bound ruthenium complex as heterogeneous catalyst for hydrogenation I: Effect of support, ligand and solvent on the catalyst performance*. *Chinese Journal of Chemistry*, 2006. **24**(7): p. 840-844.
14. Yu, Y.M., et al., *Carbon dioxide hydrogenation catalyzed by ruthenium complexes immobilized on MCM-41*. *Journal of Fuel Chemistry and Technology*, 2006. **34**(6): p. 700-705.
15. Morgan, G.G., et al., *Tethering of Dinuclear Complexes to SBA-15 and Their Application in CO<sub>2</sub> Hydrogenation*. *ChemCatChem*, 2013. **5**(4): p. 951-958.
16. Zhou, G., et al., *Effects of structure on the carbon dioxide methanation performance of Co-based catalysts*. *International Journal of Hydrogen Energy*, 2013. **38**(24): p. 10012-10018.
17. Kiatphuengporn, S., M. Chareonpanich, and J. Limtrakul, *Effect of unimodal and bimodal MCM-41 mesoporous silica supports on activity of Fe-Cu catalysts for CO<sub>2</sub> hydrogenation*. *Chemical Engineering Journal*, 2014. **240**: p. 527-533.
18. Jiang, X., et al., *Bimetallic Pd-Cu catalysts for selective CO<sub>2</sub> hydrogenation to methanol*. *Applied Catalysis B: Environmental*, 2015. **170-171**: p. 173-185.
19. Witoon, T., et al., *Effect of hierarchical meso-macroporous alumina-supported copper catalyst for methanol synthesis from CO<sub>2</sub> hydrogenation*. *Energy Conversion and Management*, 2015. **103**: p. 886-894.
20. Merkache, R., et al., *3D ordered mesoporous Fe-KIT-6 catalysts for methylcyclopentane (MCP) conversion and carbon dioxide (CO<sub>2</sub>) hydrogenation for energy and environmental applications*. *Applied Catalysis A: General*, 2015. **504**: p. 672-681.
21. Noor, A.M.Z., T. Sara, and S.S. Maizatul, *Effects of Nb promoter on the properties of Cu/ZnO/SBA-15 catalyst and performance in methanol production*, in *Key Engineering Materials*. 2016. p. 94-97.
22. Liu, X., et al., *Cu-Mo<sub>2</sub>C/MCM-41: An efficient catalyst for the selective synthesis of methanol from CO<sub>2</sub>*. *Catalysts*, 2016. **6**(5).

23. Atakan, A., et al., *Synthesis of a Cu-infiltrated Zr-doped SBA-15 catalyst for CO<sub>2</sub> hydrogenation into methanol and dimethyl ether*. *Physical Chemistry Chemical Physics*, 2017. **19**(29): p. 19139-19149.
24. Kiatphuengporn, S., et al., *Cleaner production of methanol from carbon dioxide over copper and iron supported MCM-41 catalysts using innovative integrated magnetic field-packed bed reactor*. *Journal of Cleaner Production*, 2017. **142**: p. 1222-1233.
25. Kruatim, J., S. Jantasee, and B. Jongsomjit, *Improvement of cobalt dispersion on Co/SBA-15 and Co/SBA-16 catalysts by ultrasound and vacuum treatments during post-impregnation step*. *Engineering Journal*, 2017. **21**(1): p. 17-28.
26. Liu, Q. and Y. Tian, *One-pot synthesis of NiO/SBA-15 monolith catalyst with a three-dimensional framework for CO<sub>2</sub> methanation*. *International Journal of Hydrogen Energy*, 2017. **42**(17): p. 12295-12300.
27. Bacariza, M.C., et al., *Micro- and mesoporous supports for CO<sub>2</sub> methanation catalysts: A comparison between SBA-15, MCM-41 and USY zeolite*. *Chemical Engineering Science*, 2018. **175**: p. 72-83.
28. Guo, X., et al., *Carbon Dioxide Methanation over Nickel-Based Catalysts Supported on Various Mesoporous Material*. *Energy and Fuels*, 2018. **32**(3): p. 3681-3689.
29. Liu, H., et al., *CO<sub>2</sub> hydrogenation to methane over Co/KIT-6 catalysts: Effect of Co content*. *Fuel*, 2018. **217**: p. 570-576.
30. Atakan, A., et al., *Time evolution of the CO<sub>2</sub> hydrogenation to fuels over Cu-Zr-SBA-15 catalysts*. *Journal of Catalysis*, 2018. **362**: p. 55-64.
31. Wang, X., et al., *CO<sub>2</sub> methanation on the catalyst of Ni/MCM-41 promoted with CeO<sub>2</sub>*. *Science of the Total Environment*, 2018. **625**: p. 686-695.
32. Berahim, N.H., et al. *Synthesis and Characterization of Hybrid Catalyst on SBA-15 Support for CO<sub>2</sub> Hydrogenation Reaction*. in *Journal of Physics: Conference Series*. 2018.
33. Atakan, A., et al., *Impact of the morphological and chemical properties of copper-zirconium-SBA-15 catalysts on the conversion and selectivity in carbon*



- dioxide hydrogenation*. Journal of Colloid and Interface Science, 2019. **546**: p. 163-173.
34. Mureddu, M., F. Ferrara, and A. Pettinau, *Highly efficient CuO/ZnO/ZrO<sub>2</sub>@SBA-15 nanocatalysts for methanol synthesis from the catalytic hydrogenation of CO<sub>2</sub>*. Applied Catalysis B: Environmental, 2019. **258**.
  35. Cao, H., et al., *Enhancing CO<sub>2</sub> hydrogenation to methane by ni-based catalyst with v species using 3d-mesoporous kit-6 as support*. Energies, 2020. **13**(9).
  36. Gupta, S., et al., *Engineering pore morphology using silica template route over mesoporous cobalt oxide and its implications in atmospheric pressure carbon dioxide hydrogenation to olefins*. Applied Materials Today, 2020. **19**.
  37. Paviotti, M.A., et al., *Ni mesostructured catalysts obtained from rice husk ashes by microwave-Assisted synthesis for CO<sub>2</sub>methanation*. Journal of CO<sub>2</sub> Utilization, 2020. **42**.
  38. Hongmanorom, P., et al., *Enhanced performance and selectivity of CO<sub>2</sub> methanation over phyllosilicate structure derived Ni-Mg/SBA-15 catalysts*. Applied Catalysis B: Environmental, 2021. **282**.
  39. Sun, C., et al., *Tailoring the yttrium content in Ni-Ce-Y/SBA-15 mesoporous silicas for CO<sub>2</sub> methanation*. Catalysis Today, 2021. **382**: p. 104-119.
  40. Su, Y., et al., *Tungsten-containing MCF silica as active and recyclable catalysts for liquid-phase oxidation of 1,3-butanediol to 4-hydroxy-2-butanone*. Applied Catalysis A: General, 2006. **315**: p. 91-100.
  41. Wang, Z., et al., *Increasing the oral bioavailability of poorly water-soluble carbamazepine using immediate-release pellets supported on SBA-15 mesoporous silica*. International journal of nanomedicine, 2012. **7**: p. 5807-18.
  42. Bouazizi, N., et al., *Effect Of Synthesis Time On Structural, Optical And Electrical Properties Of CuO Nanoparticles Synthesized By Reflux Condensation Method*. ADVANCED MATERIALS Letters, 2014. **2015**: p. 158-164.
  43. Phul, R., et al., *Ascorbic acid assisted synthesis, characterization and catalytic application of copper nanoparticles*. 2018. **2**.

44. Musić, S., N. Filipović-Vinceković, and L. Sekovanić, *Precipitation of amorphous SiO<sub>2</sub> particles and their properties*. Brazilian Journal of Chemical Engineering, 2011. **28**: p. 89-94.
45. Zhu, S., D. Zhang, and N. Yang, *Hydrophobic polymers modification of mesoporous silica with large pore size for drug release*. Journal of Nanoparticle Research, 2009. **11**: p. 561-568.
46. Vu, T., et al., *Highly catalytic performance of novel Ni-Cu containing SBA-15 materials in the hydrodeoxygenation of guaiacol*. Biointerface Research in Applied Chemistry, 2018. **8**: p. 3339-3343.
47. Megia, P.J., et al., *Hydrogen Production from Steam Reforming of Acetic Acid as a Model Compound of the Aqueous Fraction of Microalgae HTL Using Co-M/SBA-15 (M: Cu, Ag, Ce, Cr) Catalysts*. Catalysts, 2019. **9**: p. 1013.
48. Ksiazek, M., et al., *Reduction of SiO<sub>2</sub> to SiC Using Natural Gas*. Metallurgical and Materials Transactions E, 2014. **1**: p. 272-279.
49. Yang, Y.-N., et al., *Enhanced methanol production by two-stage reaction of CO<sub>2</sub> hydrogenation at atmospheric pressure*. Catalysis Communications, 2022. **162**: p. 106373.
50. Gao, L., et al., *Synthesis of Hierarchical Nanoporous Microstructures via the Kirkendall Effect in Chemical Reduction Process*. Scientific Reports, 2015. **5**(1): p. 16061.



จุฬาลงกรณ์มหาวิทยาลัย  
**CHULALONGKORN UNIVERSITY**

## VITA

NAME	Sirimas Suelueam
DATE OF BIRTH	19 November 1997
PLACE OF BIRTH	Bangkok, Thailand
HOME ADDRESS	522, rama2 rd., Samae Dam, Bang Khun Thian, Bangkok, Thailand, 10150



จุฬาลงกรณ์มหาวิทยาลัย  
**CHULALONGKORN UNIVERSITY**